ION BEAM MIXING STUDY OF Si - Ge SYSTEM

A Thesis Submitted
in Partial Fulfilment of the Requirements
for the Degree of

MASTER OF TECHNOLOGY

by

PARITOSH CHAUDHURI

to the

MATERIALS SCIENCE PROGRAMME
INDIAN INSTITUTE OF TECHNOLOGY KANPUR
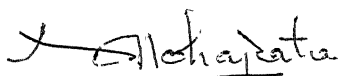July, 1993

MSP- 1983- M- CHA · ION

CERTIFICATE

It is certified that the work contained in the thesis entitled "ION BEAM MIXING STUDY OF Si-Ge SYSTEM" by PARITOSH CHAUDHURI has been carried out under our supervision and this work has not been submitted elsewhere for a degree.

Dr. Y. N. Mohapatra

Materials Science Programme,

I.I.T. Kanpur.

July 1993

Dr. V.N. Kulkarni

Department of Physics,

I.I.T. Kanpur.

July 1993

ABSTRACT

Silicon germanium alloy systems are technologically important due to their potential applications in electronic and optoelectronic devices. The present study has been undertaken to evaluate the efficacy of the Ion Mixing process to synthesize Si-Ge alloys. Three different sample configurations are utilized- 1) Ge films evaporated on crystalline silicon ii) bilayers of Si and Ge on fused quartz and iii) flash evaporated films of Si+Ge on crystalline silicon. Ion mixing has been carried out using 1 MeV Kr ions. The ion fluence is varied from $1x10^{15}$ to $6x10^{16}$ atom/cm^2. The mixing has been monitored using the Rutherford Backscattering Technique using 1.6 MeV He$^+$ ion beam. The films have been characterized using sheet resistance, SEM and EDAX measurements. The theoretical estimates of Kr ion range and its distribution has been determined using TRIM program and are compared with the experimental results.

Definite evidence of occurence of mixed layers of composition $Si_{.5}Ge_{.5}$ and typical widths of 200-500 A has been observed at the interface of Si and Ge. Samples with single Ge layer on crystalline silicon substrate show roughly linear dependence on the irradiated dose up to $1 x 10^{16}$ atoms/cm^2. The growth rate at higher fluences is seen to be considerably retarded. Further, it is inferred that shallow impurities play no role in the ion mixing mechanism. Simulation analysis of the RBS spectra indicates that there is no lateral homogeniety in the films prepared by flash evaporation. The lateral homogenity seems to improve after irradiation. In the case of the Si and Ge bilayers on SiO_2 substrates the simulation gives an oxide layer at the interface of Si and Ge films which is responsible for the hinderence of the mixing process. The theoretically calculated (TRIM) ranges of the Kr ions agree well with experimentally determined values. The experimental values of the straggling in the Kr

distribution is almost double of the calculated ones. A low temperature heat treatment ($550°C$ for 15 min in flowing dry nitrogen) is enough to improve the conductivity by two orders of magnitude indicating removal of most of the ion induced damages. For Ge films on crystalline silicon the resistivity of the film shows abrupt decrease at fluences higher than $1x10^{16}$ atoms/cm^2 even before thermal annealing. This effect indicates that ion irradiation plays a role in activating the shallow dopants in this disordered material.

ACKNOWLEDGEMENT

23July, 1993.   Paritosh Chaudhuri

CONTENTS

LIST OF FIGURES

LIST OF TABLES

CHAPTER-1

INTRODUCTION

1.1 GENERAL

The surface modification of solid can be achieved by various methods. Energetic ion beams directed under vacuum have become the most sophisticated and versatile of all methods used for surface modification of materials. Applied originally to semiconductors with considerable success such processes have now been adapted for metals, ceramics, polymers indeed the whole range of solid materials. In semiconductor industry it has been used to introduce electrically active impurities into device in controlled ways; its use continuous to expand.

The main feature of ion implantation is to introduce the foreign atoms in to a material in order to change the composition of the surface region. Ion beam irradiation can cause large change in the composition and structure of the near surface region of materials. These changes can result a variety of effects :

1) A new atomic species is added to the material (Ion implantation) [1].

2) Atoms are knocked from their original positions in collision cascades (Sputtering and Atomic mixing) [2].

3) Defects generated by irradiation can increase the thermal diffusion

coefficient (Radiation enhanced diffusion) [3].

Thus the ion implantation leads to the radiation damage i.e. production of structural defects in a material. In semiconductor industry, in general, radiation damage is not a desirable phenomena but the present annealing techniques can 'repair' this damage to a large extent. However in certain cases the ion induced damage is used to advantage in controlling carrier life time in selctive regions of the devices.

Ion beams are used to modify surfaces mainly in the following ways :
1) Direct implantation of desired species.
2) Ion Beam Mixing. The process involves use of energetic ions of heavy inert gases (Ar, Kr etc.) to induce intermixing in the pre-deposited thin films to be alloyed with a substrate.

1.2 ION IMPLANTATION AND ION BEAM MIXING (IBM)

Though the ion implantation has so many advantages like controllable addition of impurities, small lateral spread of implanted ions; but it has also some disadvantages. One of the main limitations of ion implantation is the problem of sputtering or ion induced erosion of the bombarded surface. This places an upper limit to the maximum concentration of impurities in the host, attainable by implantation and is roughly given by the ratio r/s [4]. Here r is called the preferential sputtering factor which approximates itself to values between 0.5 and 2.0 and s is the sputtering yield which is defined as the total number of target atoms

sputtered per incident projectile ion. The value of the sputteirng yield s could be as high as 20. For example, in the case of 150 keV Au implantation into Fe, the value for r is unity and s equals to 4.4.This yields a maximum Au concentration in Fe of about 25% . However for similar Au implantation into Cu, the maximum achievable concentration is only 5% . This is due to the high s value of 20 in the case of Cu [4].

The above mentioned limitation, caused by the phenomena of sputtering, can be circumvented by depositing a thin film of impurity A on the host substrate B and bombarding this bilayer configuration with energetic heavy ions [4], specially inert gas ions. The ions pass through the layers and due to the collision induced effects the atoms of the layer A tend to mix with those of layer B at the interface. The width of the mixed region increases with increase in the irradiation dose until a complete mixing of atoms of layer A and B occurs. This variation of ion implantation is commonly known as "Ion Induced Mixing", "Ion Beam Mixing" or simply "Ion Mixing". In most cases ion beam mixing has been observed to have no upper bound to the concentration of A in B [5]

The effectiveness of ion beam mixing versus direct ion implantation must presently be addressed on a case to case basis, but some studies have shown that higher alloy concentration can be achieved with high dose ion implantation. The composition of the implanted ion species as a function of depth can be adjusted by varying ion energy and dose. In contrast to ion implantation, for which maximum implanted concentration are typically limited to several atomic percent by sputtering of atoms from the surface, Ion Beam Mixing of pre deposited surface films can be used to create a wide range of carefully controllable compositions using beams of

easily generated ions. Finally Ion Beam Mixing process can be used to mix multilayer specimens in order to produce surface alloys of high solute concentration, where the implantation process is impractical. Ion Beam Mixing has therefore greatly expanded the potential applications of ion beam surface modification. Perhaps no other process is as efficient as the Ion Beam Mixing for introducing large non-equilibrium concentration of alloying elements into a wide variety of hosts [2].

1.3 CLASSES OF MATERIALS STUDIED UNDER ION BEAM MIXING

There are many applications of the Ion Beam Mixing technique have . These include silicide formation, synthesis of metastable and amorphous alloys,and enhancement in the thin film films with substrates[10]. Silicides are of considerable technological importance, especially in microelectronics where they are used as interconnects in integrated circuits. Silicides were the first systems to be studied exhaustively under ion beam mixing [6,7,8,9]. Platinum silicides studied were the first to be reported, in detail, as early as 1979 [8]. The next important class of systems studied under ion induced mixing were the metal-metal, metal-semiconductors, ceramic-metal systems and systems involving insulators like polymers [10]. Another recent study by Hoamuth et. al.[11] involved fabrication of a Y-Ba-Cu oxide film by ion induced mixing of multilayer of Y, Ba, Cu.

1.4   SILICON GERMANIUM ALLOY SYSTEM

The binary phase diagram of Silicon and Germanium system [20] shows that the two elements are   mutually miscible across the entire compositional range in conformity with the Hume-Rothery rules [21]. The relevant properties of Silicon and germanium are listed in Table 1.1.

TABLE 1.1

Element Properties	Silicon	Germanium
Atomic Number	14	32
Atomic weight	28.06	17.6
Atomic radius	1.32 Å	1.37 Å
Melting point	1410°C	940°C
Valancy	4	4
Crystal structure	Diamond structure	Diamond structure
Density	2.33 g/Cm^3	5.32 g/Cm^3
Electronegativity	1.8	1.8
Energy gap (At 300 K)	1.12 eV	0.65eV

The Si-Ge system is found to be interesting and has received considerable attention recently as a material for high speed electronic and optoelectronic devices. Any semiconductor technology based on Si-Ge alloy would be compatible with the existing Si technology. The band gap of Si-Ge alloys falls within the 1.3 μm-1.5 μm wavelength range, thereby making them

attractive for fiber optical communication applications. Many theoretical studies on the electrical and optical properties of Si-Ge heterostructure have been reported recently [12,13,14]. It has been demonstrated that $Si_{1-x}Ge_x$ alloys can be used for integrated wave guides [15] and high speed 1.3 μm detector [16]. Various schemes for efficient light emission from strained $Si_{1-x}Ge_x$ structures have also been proposed. There have been several reports on light emission from zone folded short period super lattices (SLs) which may result in a direct band gap [18].

The Si-Ge alloys can be prepared by various methods such as *thermal diffusion, Ion implantation* or *Ion beam mixing.* As described above the ion beam mixing has distinct advantages of its own. In summary it is a process in which alloys can be synthesized at considerably lower temperatures. The alloy depth can be controlled by varying the thickness of the films to be alloyed and the energy of the incident beam. The process can be used to to produce the alloy selectively on a predetermined region of a sample which is not possible by other equilibrium methods.

The ion beam mixing work on Si-Ge system has started only recently. Zhu et al [18] and Li et al [19] have reported the ion beam mixing of thin Ge marker films embedded in amorphous and crystalline silicon matrix and of multilayered structures of Si-Ge films on SiO_2. They utilized 180 keV Xe^+ ions at a constant dose of $5x10^{15}$ atoms/cm^2 to induce the mixing. Their main emphasis was to understnd the ion mixing as function of sample temperature during irradiation and to uderstand the mechanism of the ion mixing process.

To the best of our knowledge a systematic study of the dose dependence of mixing in Si-Ge system has not yet been reported. Also there

The present work has been undertaken to investigate the dose dependence of MeV Kr ion beam mixing induced in the Si—Ge system having different configrations namely i) single layer of Ge on crystalline silicon. ii) bilayers of Si anf Ge on SiO_2, and iii) Si+Ge film deposited by flash evaporation on silicon. The as deposited and irradiated films are studied using the Rutherford Backscattering Spectroscopy (RBS), Scanning Electron Microscopy (SEM), and four probe resistivity measurements to investigate the composition of mixed layers, surface microstructure and electrical properties respectively.

The experimental details of sample preparation, ion mixing, and the various characterization techniques mentioned above are described in Chapter II.

The results of backscattering experiments, SEM, EDAX and resistivity measurements on the as deposited, irradiated and thermally treated films are presented and discussed in Chapter 3. In this chapter the results of theoretical calculations of ion range and damage distribution (TRIM calculations) are also presented and compared with the experimental results.

Chapter 4 gives a summary and lists the salient conclusions of the work.

In order to make the thesis self contained the details of the ion beam mixing and RBS facility are described in two appendices at the end.

CHAPTER-2

EXPERIMENTAL

2.1. GENERAL

This chapter describes the experimental procedures and experimental arrangements. Brief outline and essential details of the various procedures about wafer polishing, wafer cleaning, Kr ion beam generation and implantation, Rutherford BackScattering (RBS) experiments, annealing etc. are given in this chapter.

2.1.1 *Substrate preparation*

Polished Si wafers and fused quartz were used as substrate for thin film deposition. The silicon substrates used were of the following types :

1) (111) n-type (phosphorus doped) of resistivity 20-50 ohm-cm and thickness 300-350 micron.

2) (111) n-type (phosphorus doped) of resistivity (1000 ohm-cm) and thickness 1000 micron.

The wafers were cut into samples of suitable sizes (2cm x 1cm). First the substrates were mechanically polished on one side under pressure using the alumina and glycerin mixture. During this lapping there is approximately 20 micron was taken off to produce a flat surface. And after

lapping the edges of the wafer were rounded to avoid the chipping off of the edges during handling. The wafers were then polished by the diamond powder to obtain a shining mirror finish.

2.1.2 Annealing Process

The lapping and polishing process which use diamond powder introduces defects in the wafer. Thermal annealing is required to recover this damage. Annealing is the thermal treatment of a damaged solid which eventually results in the recovery of crystal structure and physical properties. All the Si substrates were annealed at $800^{o}c$ for six hours. The annealing apparatus in this laboratory consists of a furnace which is electrically connected to a temperature controller, used to control or set the desired temperature. The temperature is controlled within $\pm$ $2^{o}c$. The sample to be annealed was placed in a quartz tube and put inside the furnace. Clean and high vacuum ($<10^{-5}$ torr.) was obtained in the quartz tube. The temperature of the sample was separately monitored by chromel-alumel thermocouple (fig 2.1), kept directly in contact with the sample. The samples were furnace cooled. Irradiated samples were annealed in nitrogen atmosphere.

2.1.3 Wafer cleaning

Surface cleaning of the wafer to remove the native oxide is the most important step in wafer treatment. Numerous methods of cleaning are popular in the semiconductor industry, but all have a certain common

characteristics. The first step in dealing with wafers is to thoroughly de-grease them using organic solvents such as trichloroethylene (t.c.e) followed by a thorough rinse in acetone. This cleaning procedure guarantees that any grease on wafers that might be insoluble in subsequent cleaning steps are removed. After de-greasing, etching of the residual impurities and oxide layer is to be done. Various formulations of etching solutions are available having different etching rates. The sequence of cleaning procedure followed by thin film deposition are:

1) De-greasing of wafers in trichloroethylene (t.c.e.).

2) Rinsing in acetone.

3) After drying in clean air, the substrates were briefly dipped in the etching solution of composition 2 ml HF + 15 ml HNO_3 + 5 ml CH_3COOH for half a minute using. The samples have to be handled using teflon tweezers during this process. This is called planer etch [22] with etch rate 5 μm/min. Immediately after etching the wafers were quickly immersed in distilled water to remove the residues of etching solution or to prevent further etching. This process was repeated several times till the surface oxide layer was removed.

2.1.4. Thin Film Deposition

Thin film deposition was carried out by two different processes in a vacuum less than 10^{-5} Torr.

A) Thermal evaporation :-

Fig 2.2 shows thin film deposition unit (thermal evaporation). Ge film of thickness 1550 Å , 1100 Å, were deposited on the substrate 1 and 2 respectively. In the quartz sample first Si film of thickness 1100 Å and then Ge film of thickness 1400 Å was deposited. Here the mass of Ge (M) required to obtain a film of desired thickness t was calculated on the basis of the following relation.

$$M = 2\Pi R^2.\rho.t \qquad \qquad \dots\dots(2.1)$$

where ρ is the bulk density of the material to be evaporated and R is the distance between the substrate and the evaporation boat. This mass of Ge was taken on Tungsten boat and evaporated on the above substrates. The evaporation was carried out under 2Π geometry i.e., under the assumption that the vapors diffuse only in a solid angle of 2Π, the thickness of the film can be measured directly by the method of frequency change of quartz crystal oscillators. The frequency of a quartz crystal is dependent upon the vibrating mass. The quartz crystal is placed on the substrate holder so that the film material deposited upon it at the same rate as upon the substrate, and the frequency change of the crystal gives the average thickness of the film. The thickness of the films were later measured by RBS technique as well. But it was found that the thickness obtained by the above equation varies by 30% . This is due to the non-adherence to the perfect 2Π geometry assumed in the above equation. These Ge films on the Si or SiO_2 substrates or in short, Si/Ge or SiO_2/Si/Ge samples were used for Ion Beam Mixing experiments.

B) <u>Flash evaporation</u> :-

      Unlike ordinary evaporation in the flash evaporation, the substance to be evaporated is not placed on the boat, and electrically heated, but it is dropped on a pre heated boat. This is advantageous in the case of sample having more than one component with different evaporation temperatures, e.g. mixture of Si and Ge. In the ordinary thermal evaporation process due to the comparatively slow heating, the component with lower melting point(Ge) gets evaporated earlier than the component having higher melting point(Si). Therefore the composition of the evaporating material is not realized in the film. On the other hand in flash evaporation, since the material is dropped in the form of a powder on a oreheated boat composite material as a whole gets evaporated, and the composition of the evaporating material might be realized in the film. Therefore we incorporated flash evaporation in our existing thermal evaporation unit. A sample holder with a movable arm was designed. It was mounted on a stand (fig.2.3) which could be manipulated externally without disturbing the vacuum. The height of the holder could be adjusted so that the material is at a proper height from the boat. (Typical height employed in the experiment being 14-15 cm). When the boat gets heated to a suitable temperature, the material was dropped on the heated boat by vibrating the stand externally. The material then gets evaporated in a flash gets deposited on the substrates.

2.2 SURFACE MODIFICATIONS BY KRYPTON ION BOMBARDMENT

The Si/Ge samples were bombarded with 1 MeV Kr$^+$ heavy ions at the Central Nuclear Facility, Department of Physics I.I.T. Kanpur. The bombardment fluences (doses) ranged from 1 x 10^{15} to 5 x 10^{16} Kr$^+$ ions/cm^2. The Central Nuclear facility houses the 2 MeV Van-de-Graaff Accelerator which provided the necessary ion beams for this work. Detail of this facility is given in Appendix A.

2.2.1. *The Heavy Ion irradiation chamber*:-

Ion bombardments on Si/Ge samples were carried out in the heavy ion irradiation chamber shown in fig. (3 13) The chamber is mounted on the usual oil diffusion vacuum system. Such a vacuum system is not good for its residual hydrocarbon impurities. Figure (3.2c) (3.4b) shows the pronounced carbon peak in the spectrum which is the indication of the hydrocarbon impurities. Figure 2.4 shows an enhancement of the carbon peak under increased fluence of Kr$^+$ irradiation. It therefore became necessary to develop clean vacuum conditions under which Ion Beam Mixing experiments could be carried out.

In the center of the chamber there is a movable sample holder on which a number of samples can be mounted and by moving the holder vertically by a predetermined amount the required sample can be introduced in the path of the Kr$^+$ ion beam. The holder is electrically isolated from the rest of the chamber by a perspex flange. A current integrator is connected to the sample holder. It measures the total charge acquired

during the irradiation. From the collected charge the dose (number of ions incident per square cm.) is calculated.

Surrounding the sample holder there is a cylinder made of aluminium sheet which has an opening for the passage of the heavy ion beam. This cylinder is maintained at a potential of nearly -260 volt relative to the grounded chamber. This arrangement is called a suppressor which inhibits the emission of secondary electrons from the sample during Kr^+ ion implantation. In the absence of such a suppressor the secondary electron emission can interfere in the measurement of total charge during the heavy ion irradiation.

The beam which enters the chamber is collimated by the stabilizing slits (fig.2.4). By the time it reaches the chamber it spreads slightly and is further collimated by an aperture, mounted just before the sample holder, of dimensions 3 mm (vertical) x 3 mm (horizontal). Thus an area of this dimension on the sample gets irradiated by the Kr^+ ion beam. Another important point needs to be added as regards the sample temperature rise during heavy ion bombardment. If the temperature rise is too high then the mixing due to thermal effects may become large enough. However at the ion current densities employed in this work viz 0.1 to 0.2 $\mu A/cm^2$ the expected sample temperature is about 20° to $30^{\circ}K$ [6].

2.2.2. *Ion Beam Analysis (Rutherford Backscattering)*

Figure 2.5 gives the details of the RBS chamber. This chamber is mounted on a diffusion pump vacuum system with a liquid nitrogen trap which yields a vacuum of the order of $1.0x10^{-6}$ Torr. This vacuum is quite adequate for the RBS work.

The samples are mounted on a sample holder (electrically isolated from the grounded chamber) which is similar to the one employed in the heavy ion irradiation chamber. A suppressor arrangement like the one used during the heavy ion irradiations is mounted in the chamber. The same current and charge measuring electronics used in the case of heavy ions is connected on the RBS chamber during ion beam analysis. On the side facing the beam, a quartz plate is fixed. The quartz plate gives out a blue glow when the $^4He^+$ beam falls on it. The purpose of this arrangement is to aid the alignment of the He^+ beam.

The $^4He^+$ beam is collimated before entering the RBS chamber by a X-Y slit arrangement to obtain a beam spot of about 1 mm x 1 mm dimensions or less. The detector is mounted at a scattering angle of 150° and subtends a solid angle of about 2.9 millisteradians at the center of the beam spot. The silicon surface barrier detector is mounted on a cylinder through which chilled water is circulated . The chilling of the detector helps in reducing the leakage currents in the surface barrier detector from 200 nA to 50 nA.

The electrical signals from the surface barrier detector were analyzed by the usual nuclear electronics and multi channel analyzer. The height of the signal gives the energy of the detected particles. A plot of the energy of the particles vs. the frequency of occurrence of the signals is called as spectrum which contains information regarding the elements and their depth distribution in the sample. In these measurements an EG&G ORTEC 142A preamplifier and PC based multi channel analyzer (MCA) were used.

2.4 RESISTIVITY MEASUREMENT

The "sheet resistance" of a semiconductor is an important aoft-measured parameter. The most commonly used technique in the semiconductor industry for measuring resistivity is the 'four-point probe method' [23]. This method is nondestructive, speedy and does not involve any elaborate preparation. Its use is directly applicable to ion implanted layers. The two point and three point probes used for measuring sheet resistance are not as suitable as the four point probe for implanted layers. The four point probe comprises four equally spaced metal probes which are pressed on to the semiconductor surface. The probes are usually set 'in line' (four collinear arrangement) but they can be at the corner of a square, the later arrangement allowing a smaller geometry. Since our irradiated portion in the sample is only a square of 3 mm.X 3 mm., so we purposely made the second type of arrangement where the probes are at the corner of a square of less than 3 mm. X 3 mm. (fig 2.5).

If the ratio of the layer thickness (X) to the probe spacing (S) is less than 0.4 than the average resistivity of an infinite thin sample in which the current flow is parallel to the surface is :

$$\rho = \left[\frac{\pi}{\mathrm{Log}_e\ 2}\ \frac{V}{I} \right] X = 4.532\ \frac{V}{I}\ X\ ,\quad \text{for 'in line' probes}$$

$$\rho = \left[\frac{\pi}{2\mathrm{Log}_e\ 2}\ \frac{V}{I} \right] X = 2.266\ \frac{V}{I}\ X\quad \text{for 'square' probes}$$

The above formula [24] can be used for calculating the resistivity of wafers and diffused and implanted layers as they meet the requirement X/S < 0.4. In the first case current (I) flowing between the outer probes and the voltage (V) measured across the inner probes, and in the second case the current flowing between adjacent probes and the voltage is measured across the other two probes.

The term in the bracket is called 'Sheet resistivity or sheet resistance (ρ_s)'. The concept of sheet resistance is very important in the study and application of thin conducting layers. It is not affected by the geometrical shape of the layer.

2.5   SCANNING ELECTRON MICROSCOPY (SEM) ANALYSIS

SEM is used to examine the surface and the near surface region of bulk materials (Surface topography). This is generally carried out by scanning a fine electron probe over the particular area of interest of the specimen. In this study the JEOL 840 Scanning Electron Microscope with EDAX facility (model KEGH) was used.

CHAPTER-3

RESULTS & DISCUSSIONS

3.1 GENERAL

The results of the backscattering experiments, SEM and EDAX measurements and the resistivity measurements will be presented and discussed in this chapter. The results of the TRIM calculations performed for the 1 MeV Kr^+ beam impinging on the different configurations of the Si-Ge system will also be presented. As mentioned in the previous chapter, three different configurations listed below have been used in the present study of Ion Mixing of the Si-Ge system.

Configuration I : Single Ge layer on crystalline silicon substrate.

    1.   High resistivity (111) Si (substrate)/Ge (1100 Å)

    2.   Low resistivity (111) Si (substrate)/Ge (1550 Å)

Configuration II: Bilayer of Si and Ge on SiO_2 (fused quartz) substrate

    3. SiO_2 (substrate)/Si(1100 Å)/Ge (1400 Å)

Configuration III : Flash evaporated Si+Ge on Silicon substrate.

    4.   Low resistivity (111) Si (substrate)/ (Si+Ge) 1400 Å

3.2 RBS MEASURMENTS

The results of the RBS measurements performed on the above mentioned configurations of the Si-Ge system in the as evaporated condition, after ion beam mixing and thermal treatments are presented in the following subsections.

3.2.1   RBS MEASURMENTS :CONFIGURATION I

RBS results of Ge film on low resistivity silicon substrate

The experimental RBS spectrum of the as-evaporated Ge film on silicon substrate is shown in fig. 3.1 (circles). The experimental details are already discussed in Chapter 2. The surface positions of Ge, Si and O are shown by arrows. The continuous curve indicates the simulated RBS spectrum obtained using the layer structure mentioned in the figure. The simulated spectrum shows a good visual fit to the experimental spectrum suggesting that layer structure used in simulation represents the actual sample structure. From the simulation analysis the following information is obtained :

i.)   thickness of Ge film is   1550 $\overset{o}{A}$

ii.)   presence of a thin (150 $\overset{o}{A}$) SiO_2 layer at the interface
        of the Si substrate and the Ge film.

iii.)   there is no interaction between Si substrate and Ge during
        the evaporation process.

The RBS spectra showing the the effect of the 1 MeV Kr^+ ion irradiation on the above sample are given in fig. 3.2a-c for different irradiated doses. For low dose irradiations namely 1×10^{15} and 5×10^{15} Kr^+ ions /cm^2 the expanded view of the Ge signalsis shown in fig. 3.2a-b. The mixing effect is indicated by the appearance of the Ge signals at lower energies for the irradiated sample as compared with the ones for the as evaporated sample. The effect of the irradiation is clearly seen for the ion fluence of 5×10^{15} Kr^+ ions/cm^2. Fig. 3.2(b) shows the effect of ion mixing for fluences of 1×10^{16} and 5×10^{16} Kr^+ ions /cm^2. The complete spectra including the signals for the Silicon substrate for these fluences are shown in fig. 3.2c. The comparison of the spectra in this figure shows that the Si signals also appear at higher energies indicating the migration of silicon in the top Ge film. Moreover the sharp Oxygen signal in the as evaporated spectrum is flattened after ion mixing indicating its redistribution across the mixed Si-Ge region. For the highest Kr fluence a carbon peak is also seen indicating the presence of carbon due to the cracking of hydrocarbons on the surface during ion irradiation. The presence of the implanted Kr is seen only for the higher doses of 1×10^{16} and 5×10^{16} Kr^+/cm^2 in the form of a broad peak distributed around the peak position shown by the arrow in the fig. 3.2c. The analysis of the Kr profile performed using the RUMP code gives the peak position at 6300 Å from the sample surface. The full width at half maximum (FWHM) of the Kr peak cannot be calculated accurately due to the fact that the Kr signal merges in the silicon signal. Nevertheless, we have estimated half width at half maximum (HWHM) from the visible portion of the kr signals (between channel Nos. 200 to 275). The HWHM turns out to be approximately equal to

4250 Å. This gives FWHM of the Kr distribution as 8500 Å. Assuming a Gaussian distribution of Kr atoms in the matrix the straggling of the peak distribution is estimated to be 3609 Å. These figures will later be compared with the theoretical calculations (TRIM calculations). The total number per sq. cm. of the Kr atoms retained in the sample is calculated from the area under the Kr signals. The retained Kr amount thus calculated from the RBS spectrum is within 30% of the implanted Kr dose expected from the current integration done during the irradiation.

The thickness of the mixed Si-Ge region across the interface has been calculated for different irradiation doses by simulating the experimental RBS spectra of ion mixed regions using suitable layer structure for simulations. The result of the simulation analysis is given in figures 3.3 and 3.4. The simulated curves in these figures match satisfactorily with the experimental spectra. The layer structure used for each case is shown in each figure. The mixed layer exhibits a composition of $Si_{0.5} Ge_{0.5}$ with some amount of oxygen in it. Note also that apart from the distinct layer having the above mentioned composition across the interface, the simulation also indicates a gradual increase in the Si concentration in the entire Ge film. The thickness of the mixed Si-Ge layer across the interface as a function of dose is given in Table 3.1. The concentration of the Si in the top Ge layer obtained as a function of irradiated fluence is given in Table 3.2.

TABLE - 3.1

Dose (Kr^+/cm^2)	Thickness of the mixed layer $Si_{0.5}Ge_{0.5}$	
	Low Resistive Substrate	High Resistive Substrate
1×10^{15}	200 Å	250 Å
5×10^{15}	350 Å	350 Å
1×10^{16}	420 Å	400 Å
5×10^{16}	500 Å	400˙ Å

TABLE - 3.2

Dose $(Kr \text{ ions}/cm^2)$	Conc. of Si in the top Ge layer	
	Low Resistive Substrate	High Resistive Substrate
1×10^{15}	---	---
5×10^{15}	0.03	0.04
1×10^{15}	0.04	0.07
5×10^{15}	0.04	0.11

RBS results of Ge film on High resistivity Silicon substrate

The RBS spectrum along with simulated curve for the Ge film in the as evaporated condition is shown in fig. 3.5 and fig. 3.6 show specta after irradiation with 1 MeV Kr^+ for different fluences. The simulation analysis is presented in figures 3.7 and 3.8 In this case the thickness of

the as evaporated Ge film is 1100 Å. The thickness of the mixed region of Si and Ge having a composition $Si_{0.5}Ge_{0.5}$ for the different irradiation fluences are given in these figures. The results of the analysis are given in Table 3.1 and Table 3.2.

3.2.2   RBS MEASUREMENTS : CONFIGURATION II

RBS Results of the Si-Ge Bilayers on SiO_2 substrate

The experimental RBS spectra along with the simulated curves are presented in figures 3.9, 3.10 and 3.11. Simulation for the spectrum of the as evaporated sample gives the following information :

1. Thickness of Ge layer: 1400 Å

2. Thickness of Si layer: 1100 Å

3. 700 Å of oxide layer at the Si/Ge interface.

There is no appreciable mixing at lower doses of $1x10^{15}$ and $5x10^{15}$ Kr^+ ions/ cm^2 (fig. 3.10). However, mixing is clearly seen for the ion fluences of $1x10^{16}$ and $5x10^{16}$ Kr^+ ions/cm^2 (fig. 3.11). It is also seen that the oxygen peak is flattened at the highest dose. A small peak is also observed at the surface energy position of carbon.

3.2.3   RBS MEASUREMENTS : CONFIGURATION III

RBS Results of the Flash evaporated Si+Ge layer on Si substrate

The RBS spectrum of the flash evaporated film of Si-Ge on low resistivity Si substrate is shown in figures 3.12 and 3.13. The flash

evaporation was performed to achieve a film having a homogeneous composition of $Si_{0.5}Ge_{0.5}$. From the backscattering spectrum it appears that the Si and Ge in the film do not posses a uniform composition. From the area under the peaks of Ge and Si the number of Ge and Si atoms turn out to be $3.2x10^{17}$ at./cm^2 and $1.8x10^{17}$ at./cm^2 respectively. This gives an average composition of $Ge_{0.64}Si_{0.36}$ for the as deposited film. The simulated curve obtained using this composition suggests that the film thicknes is 1400 Å. The simulated curve is shown by the continuous line in fig. 3.13a. for comparison purpose. It was not possible to obtain a layer structure which could yield a satisfactory fit to the experimental backscattering spectrum after simulation. We therefore feel that the film components are not homogeneously mixed and especially there is a lateral inhomogeneity in the film composition. However we do not have a direct experimental evidence in support of the above argument.

The effect of Kr irradiation after the fluences of 2, 4, and $6x10^{16}$ atoms/cm^2 is shown by the RBS spectra in fig. 3.12 and 3.13b. A gradual flattening of the Si signal is seen to occur which indicates that the composition is becoming more and more homogeneous. The signals from the implanted Kr are also seen to appear between channel numbers 200 and 250 fig 3.12. This is a part of the total Kr distribution which is Gaussian in nature with a peak at channel number 225 and whose signals at energies below 1 MeV and above 1.18 MeV are mixed up with the RBS signals coming from Si and Ge respectively.

The RBS spectrum obtained after irradiation of the highest Kr dose (6×10^{16} atoms/cm^2) for this sample is shown in fig. 3.13b. For

comparison a simulated spectrum obtained using the layer structure indicated in the figure is also shown. Apart from the effect of homogenization in the film composition, it is also evident that the Ge has mixed with the substrate Si which is exhibited by a low energy tail in the Ge signals extending down to the channel number 250.

3.3. SEM AND EDAX MEASURMENTS

The samples of type III configurations (flash evaporated Si+Ge on low resistivity silicon) have been studied by scanning electron microscopic technique to investigate the effect of irradiation on the surface topography.

The SEM pictures of the flash evaporated film in the as deposited condition and after Kr^+ irradiation at $4x10^{16}$ ions/cm^2 and $6x10^{16}$ ions/cm^2 are shown in fig.3.14. The surface of the film just after deposition is plain and does not exhibit any significant features. The EDAX analysis (see Table 3.3) gives the composition of the the film as $Si_{.78}Ge_{.22}$ Note that this composition is quite different from that obtained from the RBS analysis. This is due to the fact that the EDAX measurements probe to much larger depths and give the average concentration. Since the substrate is silicon it shows silicon enriched compositions in the EDAX measurements. After Kr^+ irradiation, these films develop interesting features as shown in fig.3.14b-c. It exhibits dark holes majority of which are of 0.1 μm diameter after irradiation with a dose of $4x10^{16}$ ions /cm^2. A few dark holes with larger diameter of about 1 μm are also observed. The irradiation at a higher fluence of 6×10^{16} changes the feature of the surface making the

dark and bright portions elongated as shown in the SEM picture of fig.3.14c. Also the density of the larger dark holes has been considerably reduced at this higher fluence. The results of the EDAX analysis are presented in Table 3.3. The bright portions are richer in germanium than the dark spots. The microstructural changes after irradiation seems to be due to the segregation of two different phases which are homogeneously mixed.

TABLE-3.3

Position	Atomic Composition of Si and Ge	
	Si	Ge
Si/Si+Ge (As evaporated)	78	22
Si/Si+Ge (Dose:4×10^{16} Kr^+/cm^2)		
(In Black region)	85	15
(In White region)	75	25
Si/Si+Ge (Dose:6×10^{16} Kr^+/cm^2)		
(In Black region)	84	16
(In White region)	72	28

3.4 RESISTIVITY MEASURMENTS

It is well known that ion irradiation causes various types of defects which change the resistivity of the implanted material. Normally a post implantation heat treatment is necessary to anneal out such defects. In order to study the annealing characteristics of the irradiated layers samples of configuration II (Si and Ge bilayers on amorphous SiO_2 substrate) are most suitable. This is because the substrate is insulating and therefore it does not interfer in the sheet resistivity measurements. The as deposited films shows resistivity of the order of 38 Ohm-cm. After irradiation the resistivity drops to a connsiderably lower value of Ohm-cm. The variation of the resistivity with the ion fluence is not very significant. Further on annealing at $550^{\circ}C$ for 15 min. there is a marked lowering (about two orders of magnitude) of resistivity for all the irradiation fluences. However, the annealed samples do show a systematic increase in the resistivity with increasing dose. The significant decrease in the resistivity after annealing is an indication that most of the damage has been recovered. Nevertheless the dose dependence of resistivity of annealed samples shows that the sample irradiated at higher fluences are not completely recovered. It is noteworthy that the damage recovery has occured using significantly lower temperature and relatively short time.

One of the consistent features of sheet resistivity measurments is that the as-deposited layers have higher resistivities than ion-irradiated ones. This clearly indicates that the as-evaporated layers are initially more disordered and ion implantation helps in relaxing the amorphous layer. In the relaxed structure, there is a higher possibility of

electrical activation of shallower impurities giving rise to lowering the resistivity. This is best demonstrated in sheet resistivity measurments on cofiguration I i.e, Ge layer evaporated on high resistive Si substrates shown in fig. (3.17). Even before annealing , the resistivity decreases dramatically at fluence higher than 1×10^{16} atoms/cm^2 clearly indicating the irole of ion irradiation in activating shallow impurites in this disorded material. Similar recovery occurs for samples irradiated with lower fluences only after heat treatment.

3.5   TRIM CALCULATIONS AND DOSE DEPENDENCE OF MIXING

The TRIM (TRansport of Ion in Matter) program [25,26] (version 1992) was used to estimate the range of Kr$^+$ ions, straggling in the ion range, number of displacement of target atoms and theenergy spent in the displacement of the target atom etc.

The program takes as input the incident ion mass and energy, the details of the layer structure, the displacement energy of lattice atom to its site E_d and the binding energy E_b. The program is explained in detail in reference No.[26]. If Z_1 and E_1 are the atomic number and energy of the incident ion, Z_2 is the atomic number of the target atom and E_2 is the energy of the target atom acquired after a collision event with the incident ion the following can be the consequences under different conditions :

Condition	Consequence

1. $E_1 > E_d$, $E_2 > E_d$: A vacancy results

2. $E_1 > E_d$, $E_2 < E_d$: E_2 is released in the form of phonons

3. $E_1 < E_d$, $E_2 > E_d$: Original atom remains at the site. The event is then called as "Replacement collision ".

4. $Z_1 \neq Z_2$: Z_1 becomes an antisite lattice atom

5. $Z_1 = Z_2$: Z_2 merely replaces Z_1 in the cascade and E_1 is released in the form of phonons.

6. $E_1 < E_d$, $E_2 < E_d$: Z_1 becomes an interstitial and $E_1 + E_2$ is released in the form of phonons.

The TRIM calculations were performed for the samples of type I configuration for the Ge film thickness of 1550 Å and 1100 Å on silicon substrate of 1 μm thickness. The thickness of the substrate was chosen such that the incident kr^+ ion is completed stopped in the in the defined layers. The calculationswere performed for 2000 events (incident ions) for 1550 Å Ge film while for 200 events for the 1100 Å Ge film on the silicon substrate.

The results of the TRIM calculations are shown in figures 3.16 and fig.3.17. The range of Kr ions for the case of 1550 Å Ge film on Si is about 5200 Å while for the thinner film of 1100 Å on Si it is 5600 Å. The straggling values are 1750 and 1535 Å respectively. As mentioned in section 3.2.1 above it is not possible to determine accurately the depth distribution of Kr atoms form the backscattering spectra since the Kr peak distribution is very broad and it merges with the backscattering signals

coming from the Silicon substrate as well as the top ge film. Nevertheless we have attempted to determine the depth vs. concentration profile of the Kr signal for the case of thicker Ge film (1550 Å) on silicon. To determine the profile, the simulated RBS spectrum for the irradiation dose of $6x10^{16}$ atoms/cm^2 was subtracted from the experimental spectrum fig.3.4b. Note that the layer structure used for simulated spectrum did not contain Kr distribution in it (since it is not possile to incorporate a single distribution in a multilayer structure in the present RUMP package). Therefore the signals in subtracted spectrum are considered to arise from the Kr atoms distributed in the Ge-Si layered matrix (it may be noted here that some abrupt changes occuring in the signal height , i.e. counts, have to be ignored). This subtracted spectrum is then converted in the depth vs. concentration distribution of Krypton atoms which is shown in fig.3.18.

Thus the experimentally calculated range and straggling of the Kr profile are 6300 Å and 3610 Å. The experimental value of the range is quite close to the one obtained by TRIM (theoretical calculations). On the contrary there is a large discrepancy between the experimental and theoretical value of the straggling. The experimental value of 3610 Å is two times larger than the the value obtained from the theoretical calculations (1800 Å). The comparision indicates that the peak of the distribution occurs at the expected position but the distribution is much broader. The broadening in the Kr distribution is expected to occur due to the migration of Kr atoms in the large mobile defect environment produced during the irradiation process[28]. The average displacements of the target atoms per incident ion is similar for both the Ge films (fig.3.17).

The growth of the mixed layer $Si_{0.5}Ge_{0.5}$ across the interface as a function of dose is plotted in fig.3.19 for the two cases of low and high resistivity silicon substrates. The initial grwoth in the thickness of the mixed layer increases linearly with dose. There has been no detailed studies on dose dependence of growth of mixed layers in Si-Ge systems. Although a linear dependence in the width of a thin (5 Å) Ge marker layer embedded in single crystal silicon has been reported to occur under Xe ion irradiation. [19]. Note that the growth of the mixed Si-Ge layer is similar for both the samples. Note that the TRIM calculations give similar target displacement per incident ion for both the films since the thickenesses of the two films are not very different. Also it is known that the shallow dopants do not affect the ion mixing rate of Si-Ge structures [18]. In fact it is also known that ion mixing rates of Ge in Si are independent in the presence of metallic impurities such as W, Au etc.[18]. However thermal inter diffusion rates in amorphous Si-Ge structures are known to be enhanced in the presence of shallow dopants and metallic impurities. Thus the intial part (up to the fluence of $1x10^{16}$ atoms/cm^2) of the dose dependence of the growth of the mixed layer indicates that the ion beam mixing mechanism is quite different from that of thermal diffusion.

At higher dose of $5x10^{16}$ atoms/cm^2 the rate of growth of the mixed layer is seen to have retarded considerably. Such retardation in the growth is seen for the first time and is quite surprising. The reasons of such retardation and the underlying mechanisms of inhibition of growth at larger fluences need to be investigated in detail.

For the samples of type II configuration (Si and Ge bilayers on SiO_2) the mixing is seen only for doses higher than $1 X 10^{16}$ atoms/cm^2.

This is probably due to the presence of relatively thick oxide layer at the interface of silicon and germanium films. The presence of oxide layer is borne out clearly from the simulations presented in fig. 3.9.

For the configuration III (flash evaporated Si+Ge on Silicon substrates) since the elements are finely dispersed as particles of sizes less than a micron in the layer such analyses of grwoth rate of the mixed layer cannot be carried out. The basis of the backscattering analysis is that the sample is laterally homogeneous over the entire region on which the ion beam is incident (generally 1 sq. mm). As discussed in section the RBS spectrum for these samples in the as deposited condition could not be simulated satisfactorily. On the other hand after irradiation the simulation results in much better theoretical fit to the experimental RBS profile. This indicates that the mixing is occuring in the lateral direction between different particles leading to a greater degree of homogenization in the lateral direction.

CHAPTER-4

SUMMARY AND CONCLUSIONS

The present study has been undertaken to evaluate the efficacy of the Ion Mixing process to synthesize Si–Ge alloys. Three different sample configurations are utilized-

I : Ge films evaporated on crystalline silicon of different resistivity.

II : Bilayers of Si and Ge on fused quartz

III : Flash evaporated films of Si+Ge on crystalline silicon.

Ion mixing has been carried out using 1 MeV Kr ions. The ion fluence is varried from 1×10^{15} to 6×10^{16} atom/cm^2. The mixing has been monitored using the Rutherford Backscattering Technique using 1.6 MeV He$^+$ ion beam. The films have been characterized using sheet resistance, SEM and EDAX measurements. The theoretical estimates of Kr ion range and its distribution has been determined using TRIM program and are compared with the experimental results.

The salient conclusions of the present study are :

1. Definite evidence of mixing between silicon and germanium atoms has been observed at the interface

2.. The mixed region is observed to have composition of $Si_{.5}Ge_{.5}$. with typical widths varying from 200 to 500 Å. The width of the mixed region across the interface for the type I sample with single Ge layer on crystalline silicon substrate shows roughly linear dependence on the irradiated dose up to 1 x 10^{16} atoms/cm^2. The growth rate at higher fluences is seen to be considerably retarded. No significant difference of the dose dependence of growth rate is observed on low and high resistivity silicon suubstrates. This is a pointer to the abscence of the role of the shallow dopants in the mechanism of the Ion Beam Mixing.

3. The simulation of the experimental backscateering spectrum of the flash evaporated sample in as deposited condition does not yield a good fit to the data points. This is indicative of abscence of lateral homogeniety in the films prepared by flash evaporation. The lateral homogenity seems to improve after irradiation.

4. In the case of the Si and Ge bilayers on SiO_2 substratesthe simulation gives an oxide layer at the interface of Si and ge films which is responsible for the hinderence of the mixing process.

5. The theoretically calculated (TRIM) ranges of the Kr ions agree well with experimentally determined values. The experimental values of the straggling in the Kr distribution is almost double than the calculated ones.

6. A low temperature heat treatment (550°C for 15 min in flowing dry nitrogen) is enough to improve the conductivity by two orders of magnitude indicating removal of most of the ion induced damages. For samples of type I configuration (Ge films on silicon)the resistivity of the film shows abrupt decrease at fluences higher than 1×10^{16} atoms/cm^2 even before thermal annealing. This effect shows that ion irradiation plays a role in activating the shallow dopants in this disordered material.

APPENDIX - A

THE ION BEAM FACILITY

Figure A1 shows the layout of this laboratory. The accelerator is situated in the machine room. The ion beam surface modifications and characterizations are done in the beam hall which also accomodates the switching magnet and its 200 A power supply. The accelerator and the switching magnet are controlled from the control room.

A1. THE VAN DE GRAAFF ACCELERATOR
A1.1 High voltage generation:-

The Van de Graaff accelerator,manufactured by high Voltage Engineering Corporation, is a belt type electrostatic generator, is used to develop accelerating voltages up to 2 MV. Basically the operation of the generator is very simple. If one deposites charge on the inside surface of a closed conducting shell the charge accumulates on the outside surface. Basic electromagnetic laws prevent the charges from residing anywhere inside. Inside the accelerator there exists such a shell which serves as the high voltage terminal. An insulating belt moves through this shell. Electrons are constantly removed from the belt on the side away from the high voltage terminal by applying a positive potential. This leaves a positive charge on the side of the belt moving towards the high voltage terminal. The positive charge on arriving on the inside of the high voltage

shell accumulates on its outer surface. Consequently the potential of the high voltage dome/shell rises. If not properly insulated the dome will lose its charge to the surroundings by sparking. To prevent this the whole assembly is enclosed in a pressure vessel containing an insulating Nitrogen plus CO_2 gas at about 360 psi pressure

Along the length of the accelerator a uniform potential gradient is achieved between the high voltage terminal and ground by a series combination of high value resistors called column resistors. Each column resistor is of approximately 1500 M Ω resistance.

The charge on the high voltage dome is simultaneously and continuously removed by the Corona points shown in Figure A1 and by the series combination of column resistors. The dome voltage remains fixed when the rate of deposition of charge by the belt equals that of removal by the Corona points and the column resistors. A generating voltmeter attached on the side of the accelerator pressure vessel measures the dome voltage.

A1.2 Generation of Chaged Particle:-

Accelaration of charged particle

The path followed by the charge particle beams is evacuated to about 5×10^{-6} Torr. The acceleration of these charged particles occurs in the accelerator tube shown in the Figure A1. The tube is made up of a series of alternately placed electrodes and insulating glass vertibrae. The connections are made such that one column resistor connects two electrodes of the accelerator tube. Thus there exists an uniform potential gradient inside the tube and the necessary evacuated path. The ions of the required

beam are leaked into the accelerating tube from the high voltage side. Under the potential the charged particles accelerate. The beam so generated is then focused and stabilized.

ION SOURCE, FOCUSING AND BEAM CURRENT CONTROL

The desired ion beam atoms are kept in the form of high pressure gas in gas bottles contained inside the high voltage terminal. A controlled amount of the gas is leaked into an ion source by a mechanism called a thermomechanical leak. In the ion source these gas atoms get ionised on application of a R.F. frequency voltage. The ions are repelled out of the ion source under the influence of a positive potential applied to an electrode inside the ion source. This positive potential is used to get the desired beam current. A focusing electrode is mounted just outside the ion source. The voltage applied to this electrode results in proper focusing of the ion beam.

The ion source focusing and beam current control systems cannot be powered from outside since they are placed inside the high voltage dome. They have to be run on power generated inside the high voltage dome. For the purpose of this power generation two 150 watt alternators are used. These alternators are mounted inside the pulley which supports the charging belt inside the high voltage terminal. The alternators use the belt rotation to generate the necessary power for driving the assembly inside the high voltage shell.

A2. THE SWITCHING MAGNET

The ion beam on emerging from the accelerator is steered into its appropriate ports with the help of a switching magnet. The magnet is shown in Figure A1. Currents of about 100 to 200 amperes are supplied to the magnet by the 200 ampere power supply shown in Figure A1. During operation the magnet is cooled by circulation of chilled deionised water through it.

APPENDIX - B

RUTHERFORD BACKSCATTERING SPECTROMETRY (RBS)

The RBS technique (fig B1) is widely employed for surface analysis of materials especially for thin film study. It is extensively used in the semiconductor industry for the studyof thin film and ion implantation problems. The next few paragraphs constitute a modest attempt towards describing this important research tool.

B.1. BASIC PHYSICAL CONCEPTS

In a backscattering experiment energetic light ions, such as 1 MeV to 3 MeV protons($^1H^+$) or alpha particles($^4He^+$), are impinged on the sample surface (Fig.B2). Some of these incident $^4He^+$ particles backscatter due to collisions with target atoms. The energy of the emergent $^4He^+$ ions depends on the mass of the target atom it has backscattered from and at what depth the collision event has occured. This is due to the difference in recoil energies of $^4He^+$ projectiles colliding with target atoms with differing masses and due to the energy loss process during its passage through the target material. The total number of backscattered alphas detected in a given energy range is dependent on the total number of scatterers (target atoms including impurity atoms) and the likelyhood of occurence of such a scattering event (which results in a $^4He^+$ being scattered into the detector). Further, statistical fluctuations (energy

straggling) are inherently present in the energy of the alpha particles emanating from the sample surface.

The energy of the projectile after the collision can be related to its incident energy by means of a *Kinetic Factor*(K). The probability of the scattering depends on the *Scattering cross section.* As the projectile pass through the scattering medium it suffers an average energy loss dE/dx and this leads to the concept of the *Stopping cross-section.* Finally, since there statistical fluctuations in the energy loss of a projectile as it penetrates a solid, particles entering a solid with a given energy will not have identical energies after travelling the same distance. this phenomenon is called *Energy Straggling.*

The above four basic physical concepts form the basis of RBS. The kinematic factor K leads to the ability for *mass analysis.*The scatering cross-section provides RBS with a *quantitative* capability. The stopping cross-section results in the capability for *depth analysis*and energy straggling sets limits on mass and depth resolusion.The details of these four factors are given below.

I) THE KINEMATIC FACTOR (K) :

The concept of the kinematic factor is intimately linked with the mass resolution capability of RBS. It is a measure of the recoil energy of the projectile of mass M_1 in a collision with an isolated target nucleus of mass M_2 and is defined as:

$$K = \frac{E_1}{E_0} ,$$

......(B1)

where E_0 and E_1 are respectively the incident and recoil energies of the projectile in an isolated two body collision with the target atom.

The energy and momentum conservation laws for this two body collison event yield the following expression for the kinematic factor.

$$K = \left(\frac{\left[1 - X^2 \sin^2\theta \right]^{1/2} + X \cos \theta}{1 + X} \right)^2, \qquad \ldots\ldots(B2)$$

where $X = M_1/M_2$ and θ is the scattering angle. From equation (B1) one gets the following equation

$$\Delta E_1 = E_0 \cdot \left(\frac{dK}{dM_2} \right) \cdot \Delta M_2, \qquad \ldots\ldots(B3)$$

where ΔE_1 is the difference in the recoil energy between two projectiles backscattered from target atoms with their masses separated by ΔM_2.

For a fixed projectile (fixed M_1) a change ΔM_2 results in the largest change in ΔE_1 for scattering angles close to 180^0. For $\theta = \Pi - \delta$ (δ being small) Equation (B3) reduces to

$$\Delta E_1 = E_0 \cdot \left[\frac{(1 - X)}{(1 + X)^3} \cdot \left(4(1 + X \delta^2) - \delta^2(1 - X^2) \right) \cdot \frac{M_1}{M_2^2} \right] \cdot \Delta M_2$$

$$\ldots\ldots(B4)$$

Therefore in order to obtain good mass resolution (i.e. to obtain maximum ΔE_1 for a particular ΔM_2) one must use a larger incident energy E_o (provided E_o is larger than the binding energy of the atoms to the target and lower than the limit beyond which nuclear reactions get activated), select M_1 to be as close to M_2 as possible provided $M_1 < M_2$ (Figure (B3)), make the scattering angle as close to 180^0 as possible. One further observes that mass resolution of RBS is intrinsically better for lighter target atoms (small M_2).

II) THE SCATTERING CROSS SECTION (σ)

The differential scattering cross section denoted by $d\sigma/d\Omega$ is defined as:

$$\left(\frac{d\sigma}{d\Omega} \right) = \frac{1}{N.t} \cdot \frac{1}{Q} \cdot \left(\frac{dQ}{d\Omega} \right) , \qquad \ldots\ldots (B5)$$

Where $N.t$ is the total areal density (number of atoms per unit area) seen by the incident $^4\text{He}^+$ beam, N is the total number of target atoms per unit volume, Q is the total number of $^4\text{He}^+$ projectiles incident on the target during RBS analysis and $d\Omega$ is the solid angle subtended by the detector at the analysis spot on the target.

The quantity dQ/Q is the probability of occurence of a collision between the projectile and the target atom resulting in the scattering of the projectile into the detector solid angle $d\Omega$ situated at the scattering angle θ. The expression given in the next page for the differential

scattering cross section is called Rutherford's formula.

$$\left(\frac{d\sigma}{d\Omega} \right) = \left(\frac{Z_1 \cdot Z_2 \cdot e^2}{4\,E} \right)^2 \cdot \frac{4}{\sin^4 \theta} \cdot \frac{\left(\left[1 - x^2 \sin^2\theta \right]^{1/2} + \cos\theta \right)^2}{\left[1 - x^2 \sin^2\theta \right]^{1/2}}$$

$$\dots\dots(B6)$$

The validity of this expression lies in the domain where the distance of closest approach of the projectile and the target nucleus is large compared with the nuclear dimensions but small compared with the Bohr radius $a_o = 0.53$ A^o .

If one considers a detector of finite solid angle Ω then the probability of a successful scattering event is described by the integral scattering cross section defined by

$$\Sigma = \int_\Omega \left(\frac{d\sigma}{d\Omega} \right) d\Omega \qquad \dots\dots(B7)$$

The typical values of the detector solid angles are normally of the order of a few millisteradians. The average differential scattering cross section is defined as:

$$\sigma = \frac{\Sigma}{\Omega} \qquad \dots\dots(B8)$$

and for small detector solid angles Ω, which one encounters in most RBS set-ups, $\sigma \longrightarrow d\sigma/d\Omega$. Thus for our purpose $d\sigma/d\Omega$ and σ are interchangeable.

Thus for the situation with small Ω equation (B5) reduces to

$$A = \sigma \cdot \Omega \cdot Q \cdot Nt \qquad\qquad \ldots\ldots (B9)$$

The scattering cross section is proportional to Z_1^2, inversely proportional to the square of the projectile energy and roughly inversely proportional to the fourth power of Sin $(\theta/2)$. The optimmum parameters must be chosen accordingly.

It should be noted that many of the conditions for maximization of respectively the kinematic factor and the scattering cross section compete with each other and therefore some compromise has to be made in choosing these parameters.

III) THE STOPPING CROSS SECTION

The stopping cross section ϵ is defined as

$$\epsilon = \frac{1}{N} \left(\frac{dE}{dx} \right) , \qquad\qquad \ldots\ldots (B10)$$

Where N being the number of target atoms per unit volume and dE/dx is the rate at which energy is lost by the projectile as it moves through the target material. ϵ can be fatorised as

$$\epsilon = \epsilon_n + \epsilon_e \qquad\qquad \ldots\ldots (B11)$$

The term ϵ_n is due to the energy loss due to collisions with the nuclei of target atoms while ϵ_e is the contribution due to the more continuous energy loss of the projectile to the electrons in the target.

For the cases in which atoms in the target exists in the form of molecules of the type $A_m B_n$ (i.e. consisting of m atoms of element A and n atoms of element B), the molecular stopping cross sections can be expressed as:

$$\epsilon^{AB} = (\; m \; \epsilon^A + n \; \epsilon^B \;) \qquad \qquad \ldots\ldots(B12)$$

ϵ^A and ϵ^B are the stopping cross sections for the elemental targets of A and B atoms respectively. This relation is called the "principle of additivity of stopping cross sections" or "Bragg's Rule."

IV) ENERGY STRAGGLING

The projectiles moving through matter lose energy due to ineractions with the individual nuclei as well as with the electron clouds. The energy loss through collisions with the nuclei are violent and discrete. There are statistical fluctuations associated with such a process. Therefore particles incident on a thin slice of thickness ΔX of the target material will emerge out, on passing through ΔX, with differing energies. These statistical fluctuations in the energy of the backscattered particles is referred to as energy straggling. Straggling leads to an impairment of mass and depth resolution of RBS.
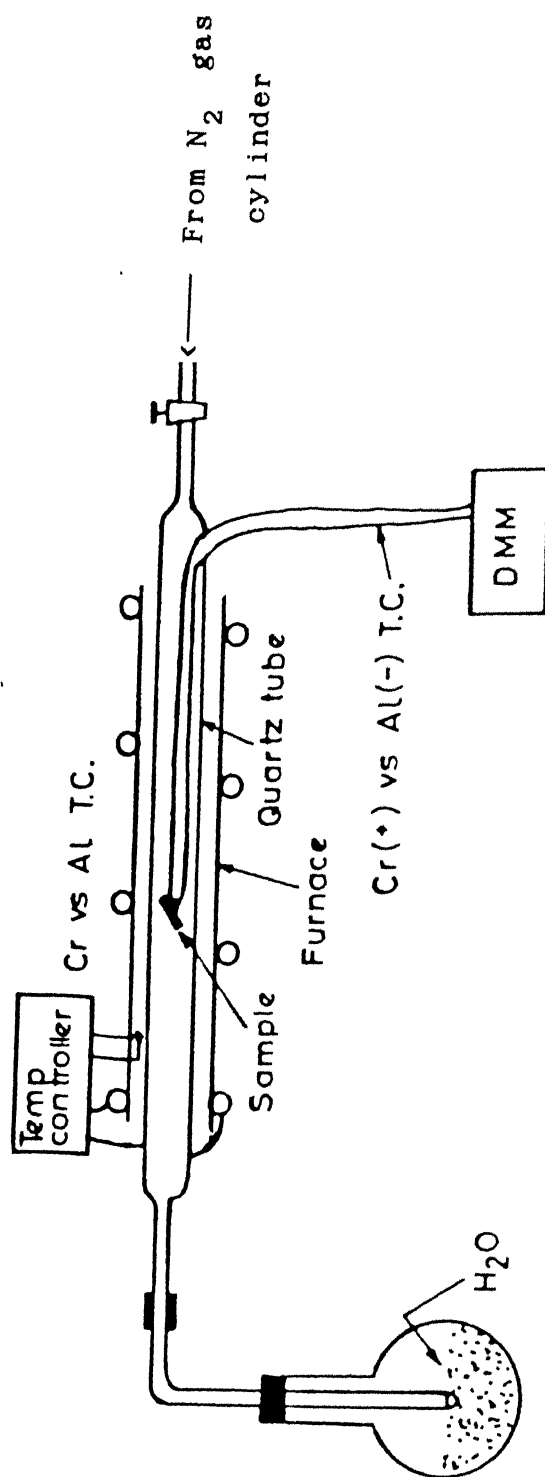
FIG. 2.1 Experimental arrangements for annealing the sample

SUBSTRATE HOLDER

GLASS DOME

TUNGSTEN BOAT

RUBBER GASKET

BASE PLATE

BACKING VALVE

AIR ADMITTANCE VALVE

ROUGHING VALVE

LIQUID NITROGEN TRAP

BAFFLE VALVE

AIR ADMITTANCE VALVE

GAS INLET

WATER CIRCULATION TUBES

THERMOCOUPLE GAUGE-HEAD

SILICONE OIL

DIFFUSION PUMP HEATER

DIFFUSION PUMP

ROTARY PUMP
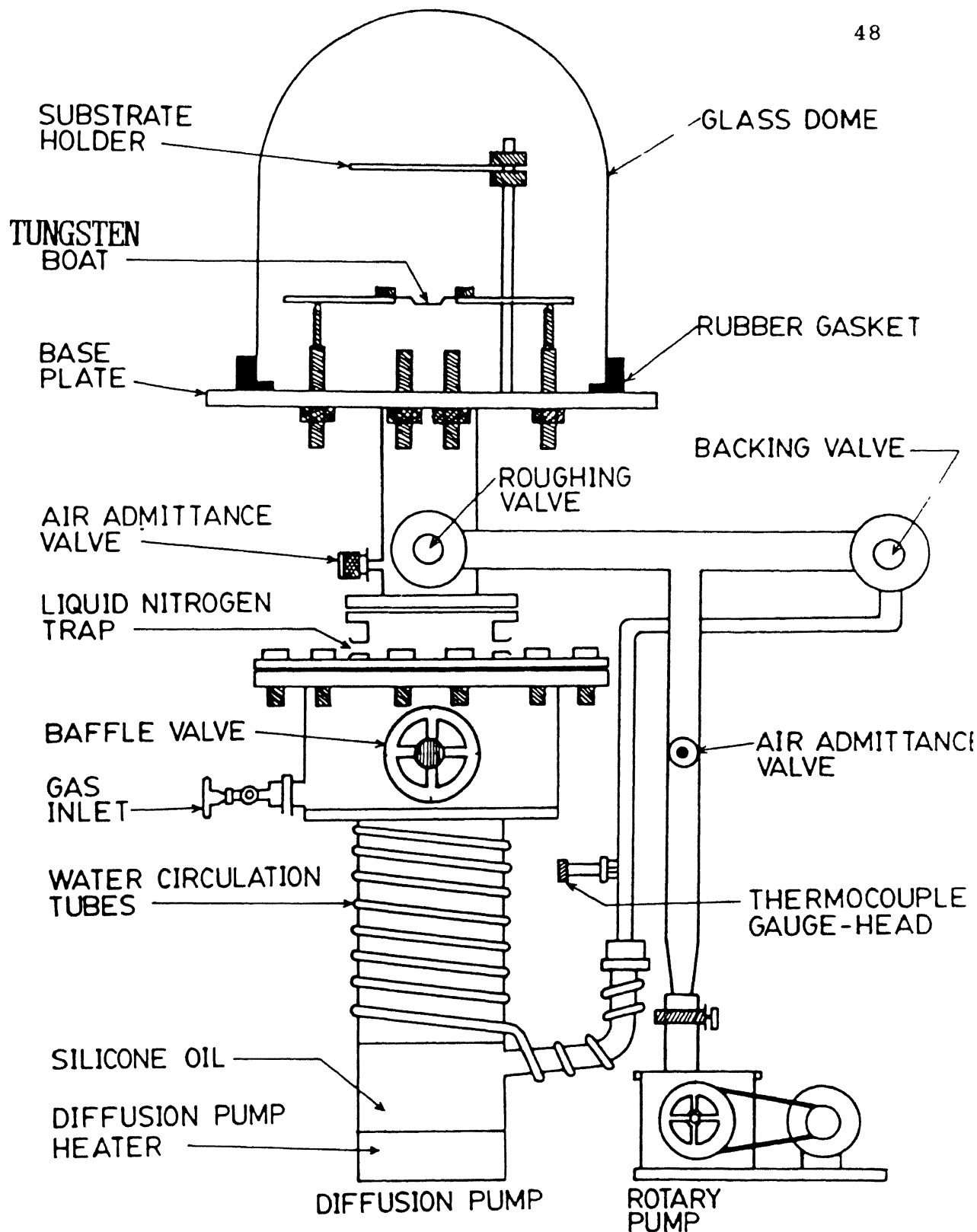
FIG 2.2 THERMAL-EVAPORATION SET-UP

SUBSTRATE HOLDER

HOPPER FOR
SAMPLE POWDER

BOAT

GLASS DOME

VACUUM
PUMP
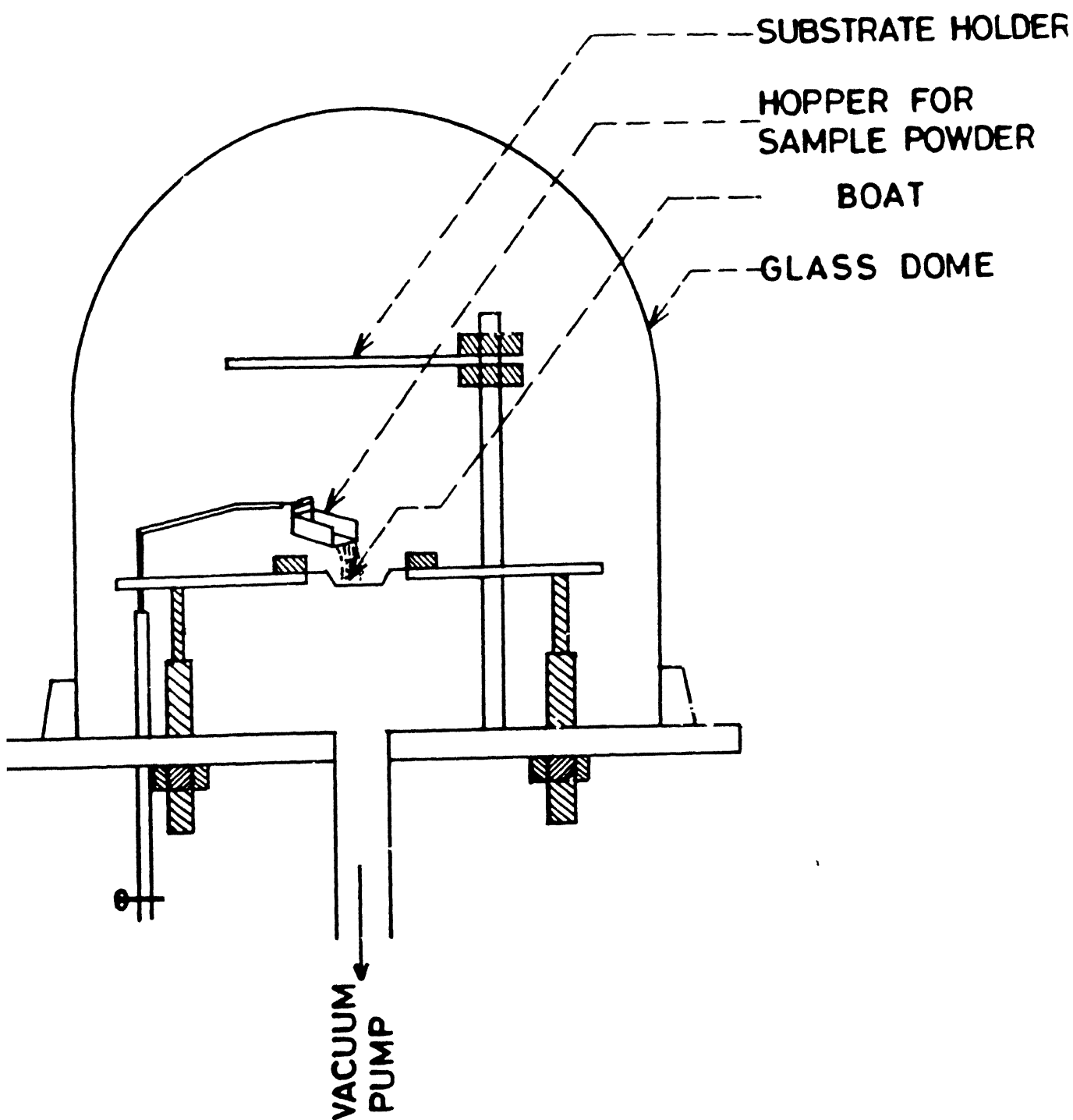
FIG 2.3   FLASH EVAPORATION SET-UP

MOVEABLE SHAFT

PERSPEX
INSULATING
FLANGE

MOVEABLE SAMPLE
HOLDER/LADDER

SUPRESSOR

QUARTZ
WINDOW

1 MeV Kr⁺ BEAM

APERTURE

3mm×3mm BEAM
SPOT

SAMPLE UNDER
IRRADIATION

FLAT
TABLE

BELLOW

● - CROSS SECTION OF
    O-RINGS

NOT DRAWN TO SCALE

TO DIFFUSION PUMP

FIG. 2.4 THE HEAVY ION IRRADIATION CHAMBER
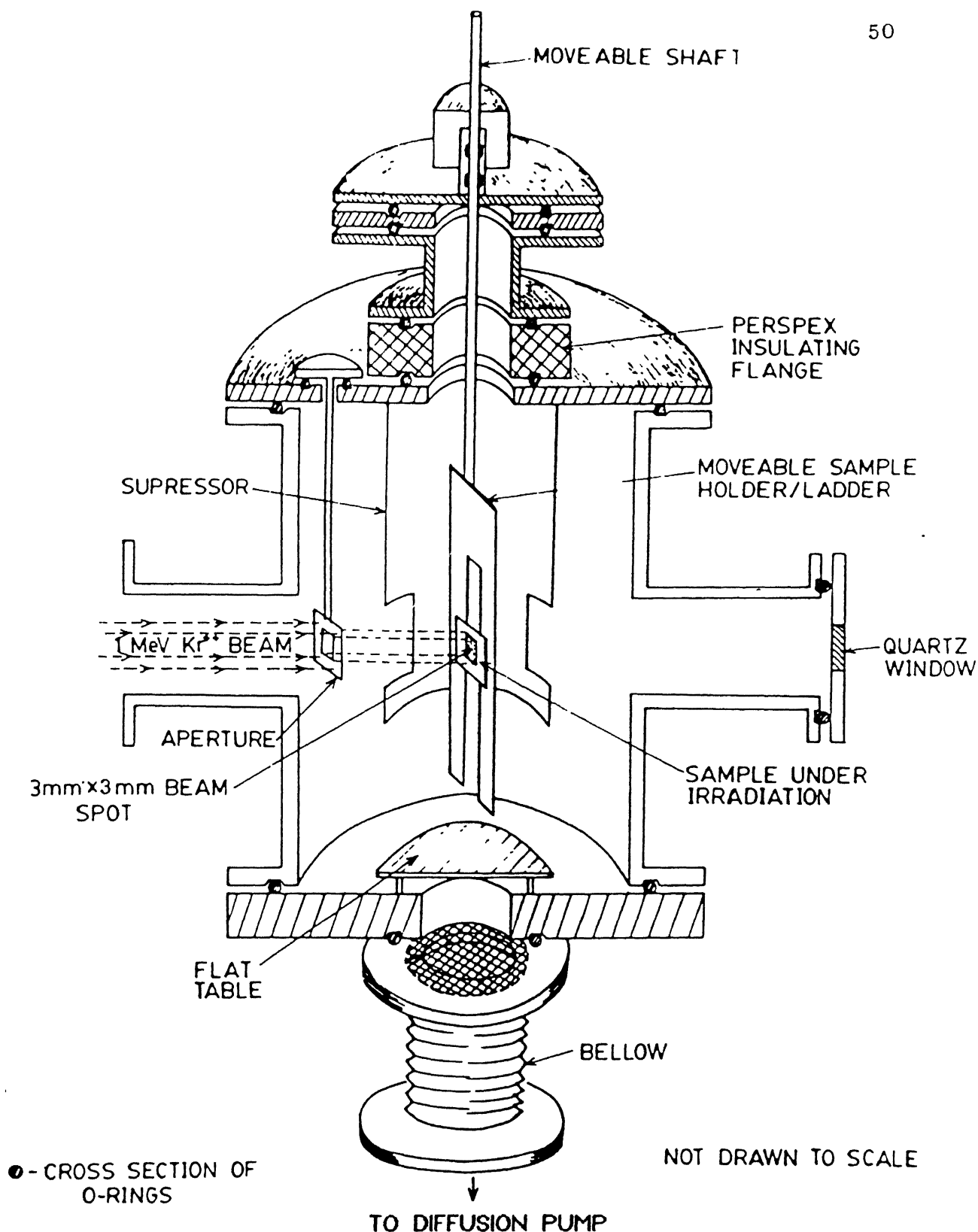
IN LINE
PROBES

SQUARE
PROBES

SEMICONDUCTOR
WAFER
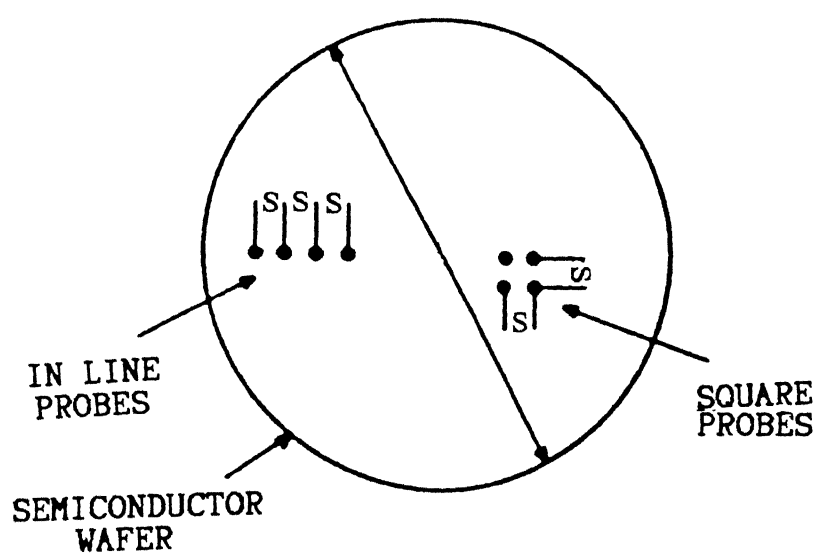
FIG 2.5   The layout of 'in-line' and 'square' four point probe geometries. 'S' is the probe spacing.
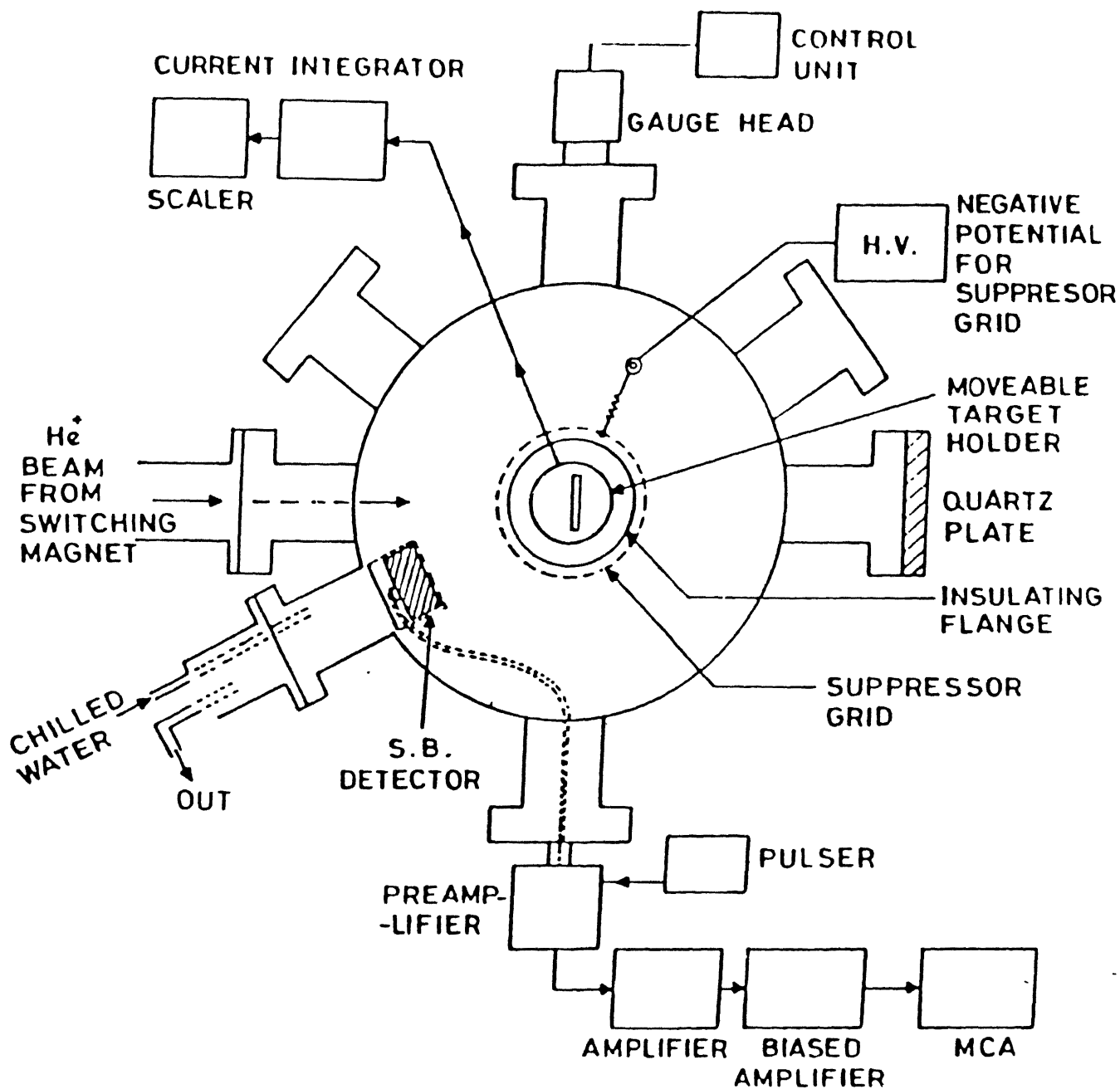
FIG 2.6   The Rutherford Backscattering Spectrometry chamber.
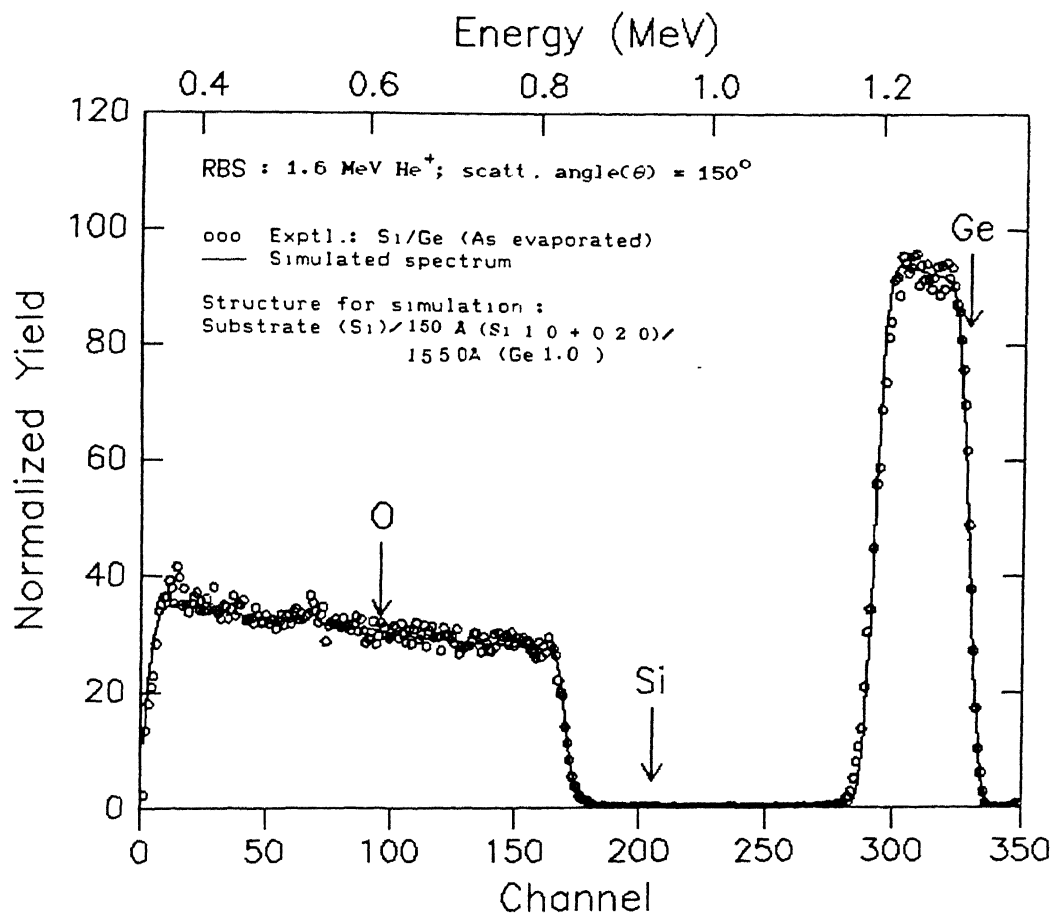
Fig. 3.1   RBS spectra of Si/Ge   (As evaporated).
(Low resistive Si)
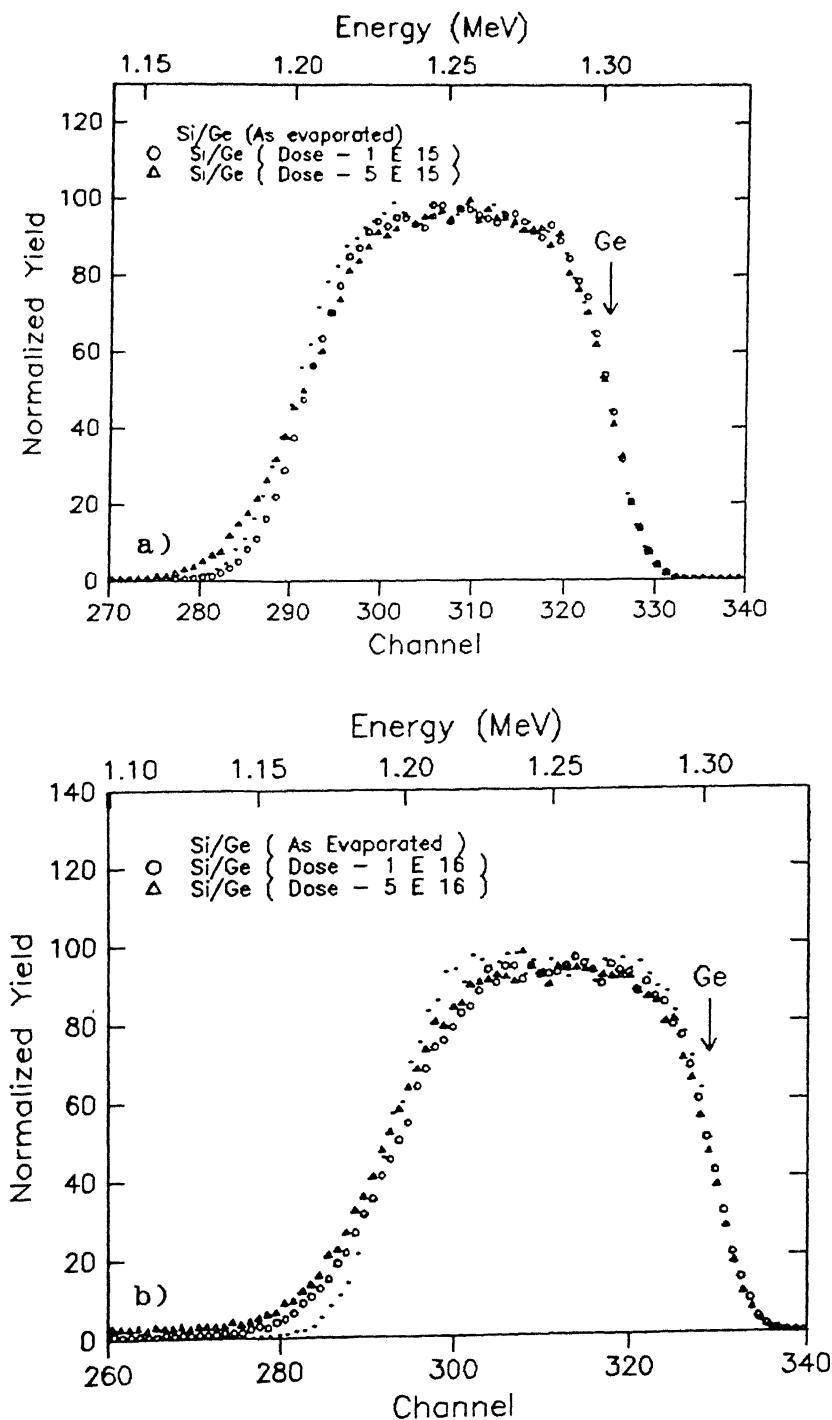
Fig. 3.2 Portion of RBS spectra of Si/Ge(1550Å) showing effect

of ion irradiation in Ge region.

a) Dose: 1×10^{15} Kr^+/Cm^2 and 5×10^{15} Kr^+/Cm^2.
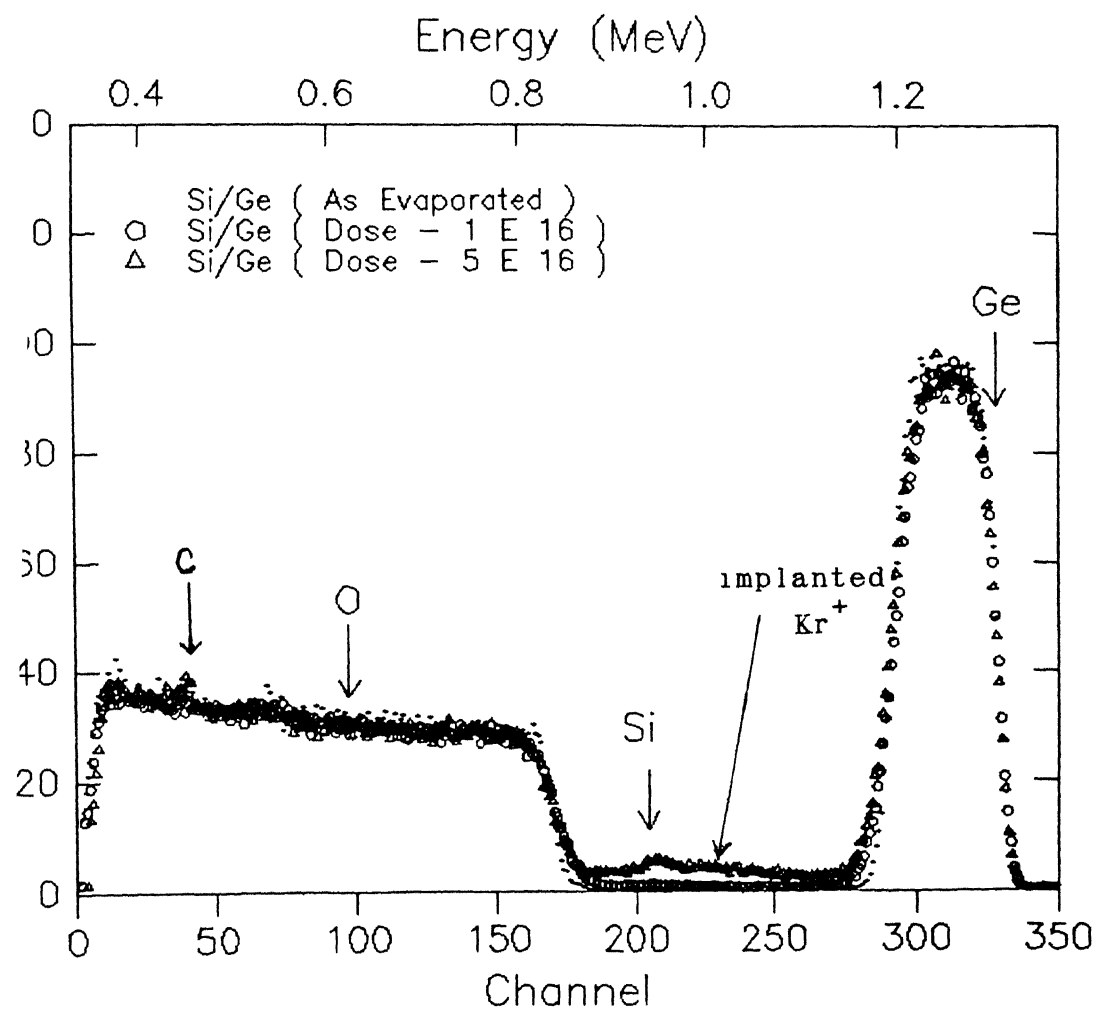
Fig. 3.2   c) Full RBS spectrum of Si/Ge(1550a)

of doses $1x10^{16}$ Kr$^+$/Cm^2 and $5x10$ Kr$^+$/Cm^2.
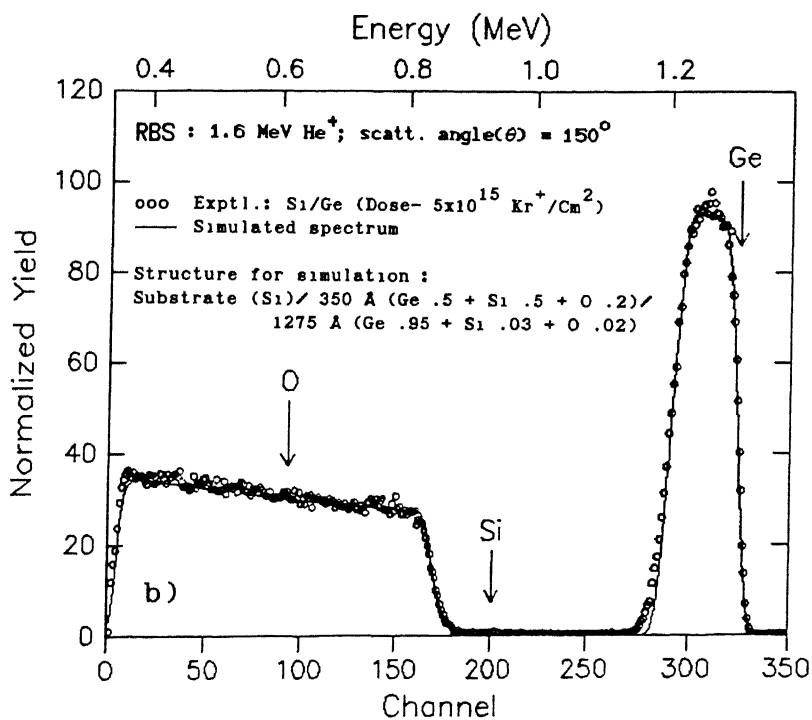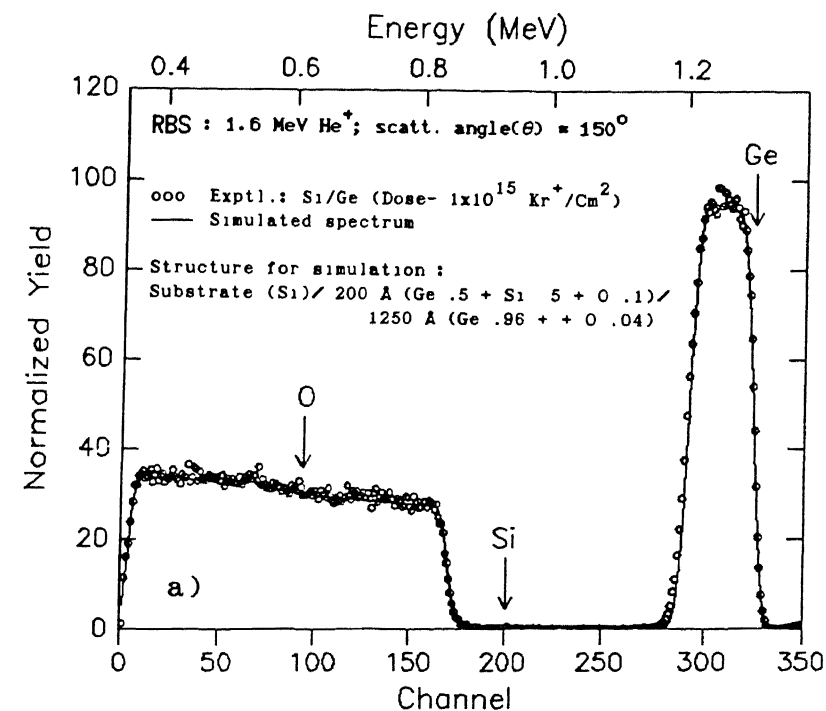
Fig 3.3   RBS spectra of Si/Ge   a) Dose- 1×10^{15} Kr^+ ions/cm^2
          (Low resistive Si)   b) Dose- 5×10^{15} Kr^+ ions/cm^2.
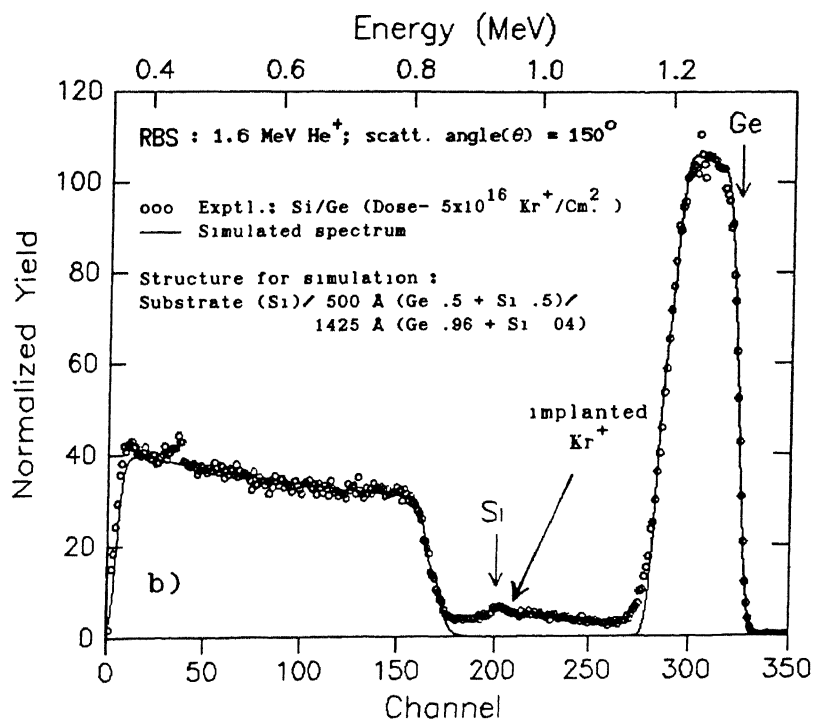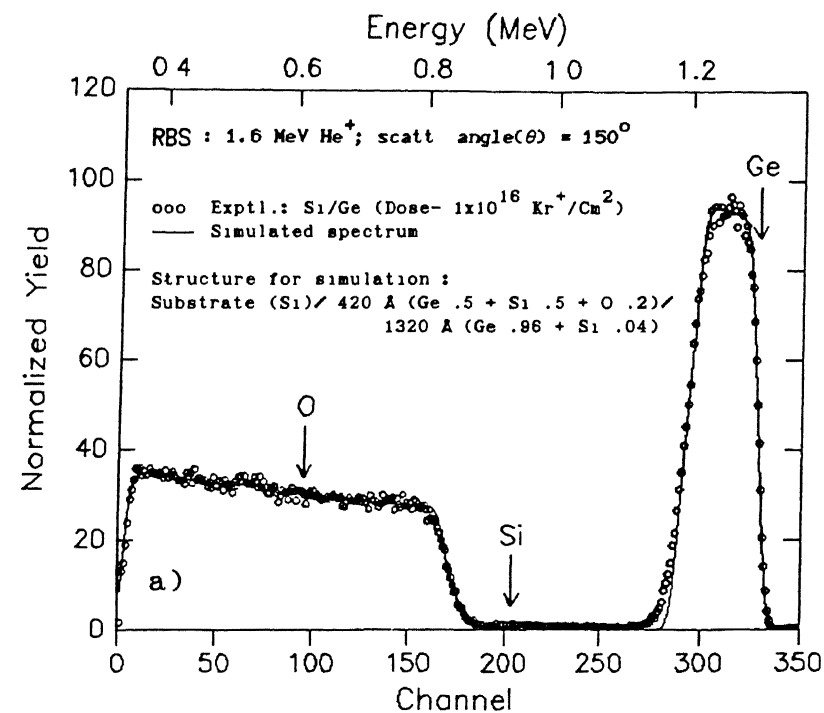
Fig 3.4   RBS spectra of Si/Ge   a) Dose- 1×10^{16} Kr^+ ions/cm^2
           (Low resistive Si)   b) Dose- 5×10^{16} Kr^+ ions/cm^2
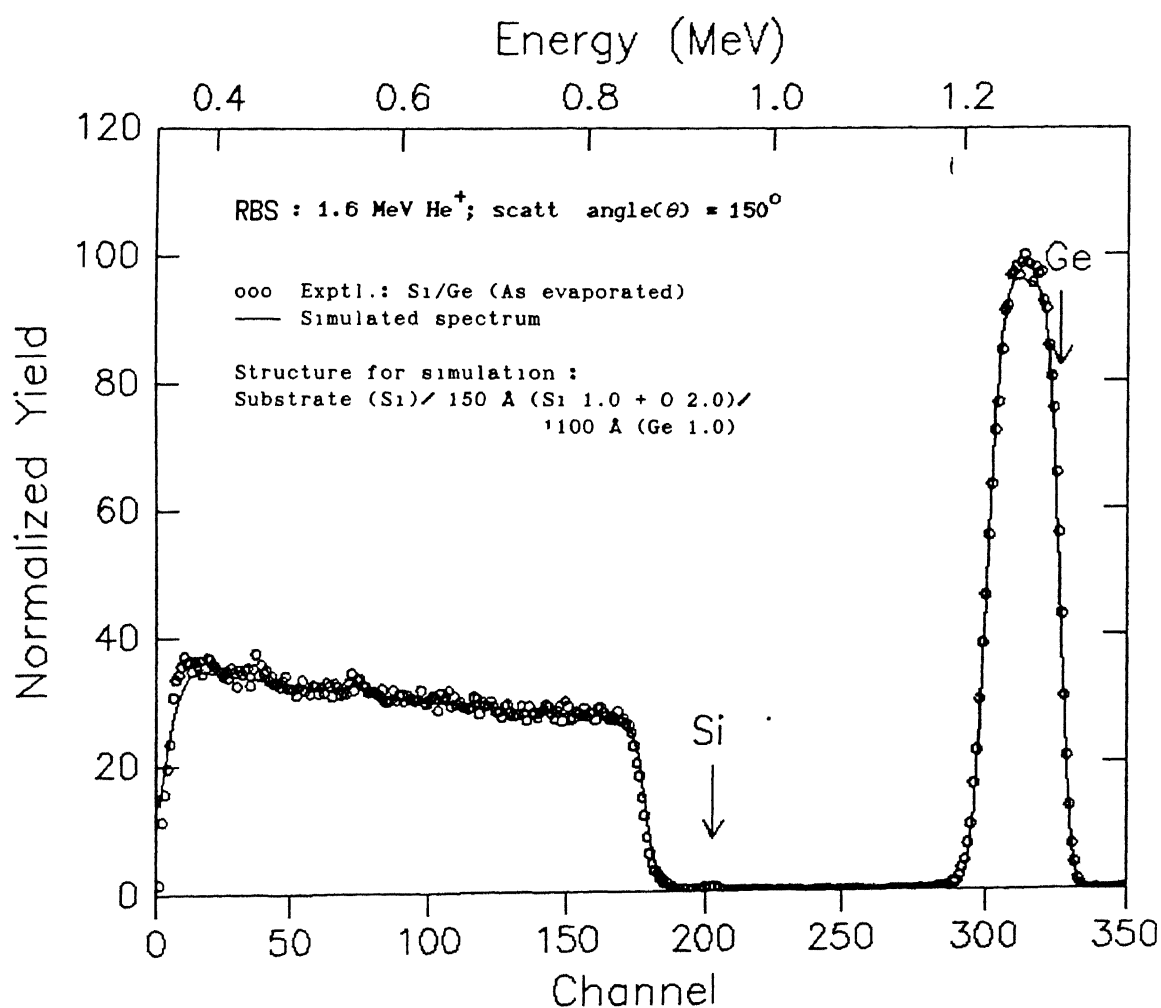
Fig. 3.5 RBS spectra of Si/Ge (As evaporated). (High resistive Si)
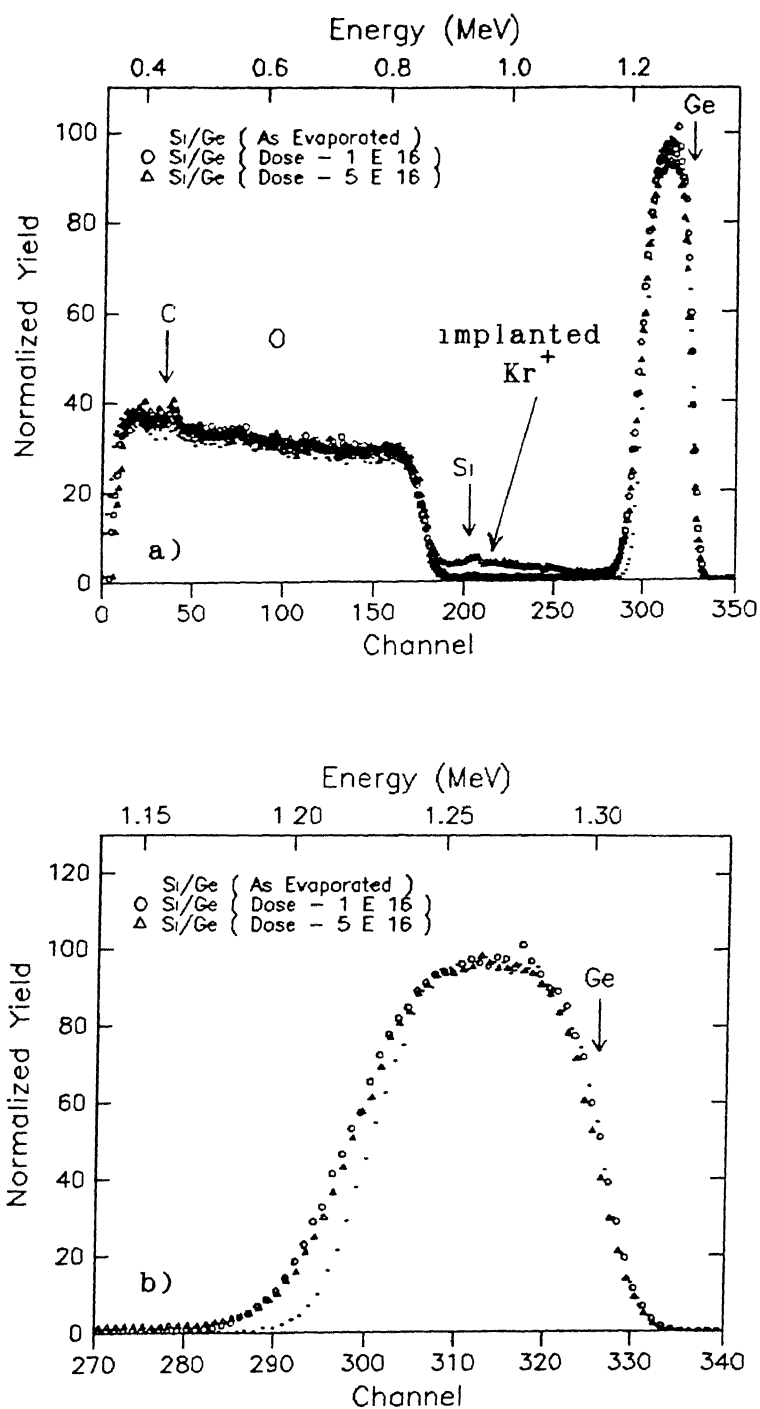
Fig. 3.6 RBS spectra of Si/Ge(1100Å) showing effect of ion irradiation

a) Full portion   b) Extended portion.

Fig 3.7   RBS spectra of Si/Ge a) Dose- 1×10^{15} Kr^+ ions/cm^2
(High resistive Si)   b) Dose- 5×10^{15} Kr^+ ions/cm^2

Energy (MeV)

0.4   0.6   0.8   1.0   1.2

RBS : 1.6 MeV He$^+$; scatt. angle(θ) = 150°

Ge

ooo   Exptl : Si/Ge (Dose- 1x10^{16} Kr$^+$/Cm.^{2})
—— Simulated spectrum

Structure for simulation :
Substrate (Si)/ 420 A (Ge .5 + Si .5 + O.15)
                1000A (Ge .93 + Si 07)

O

Si

a)

Normalized Yield

120 100 80 60 40 20 0

0   50   100 150 200 250 300 350

Channel

Energy (MeV)

0.4   0.6   0.8   1.0   1.2

RBS : 1.6 MeV He$^+$; scatt. angle(θ) = 150°

Ge

ooo   Exptl.: Si/Ge (Dose- 5x10^{16} Kr$^+$/Cm.^{2})
—— Simulated spectrum

Structure for simulation :
Substrate (Si)/ 320 A (Ge .5 + Si .5)/
                1000 A (Ge .89 + Si .11)

implanted
Kr$^+$

Si

b)

Normalized Yield

120 100 80 60 40 20 0

0   50   100 150 200 250 300 350

Channel

Fig 3.8   RBS spectra of Si/Ge   a) Dose- 1x10^{16} Kr$^+$ions/cm^2
           (High resistive Si)   b) Dose- 5x10^{16} Kr$^+$ ions/cm.^{2}

Fig. 3.9 RBS spectra of SiO /Si/Ge (As evaporated)
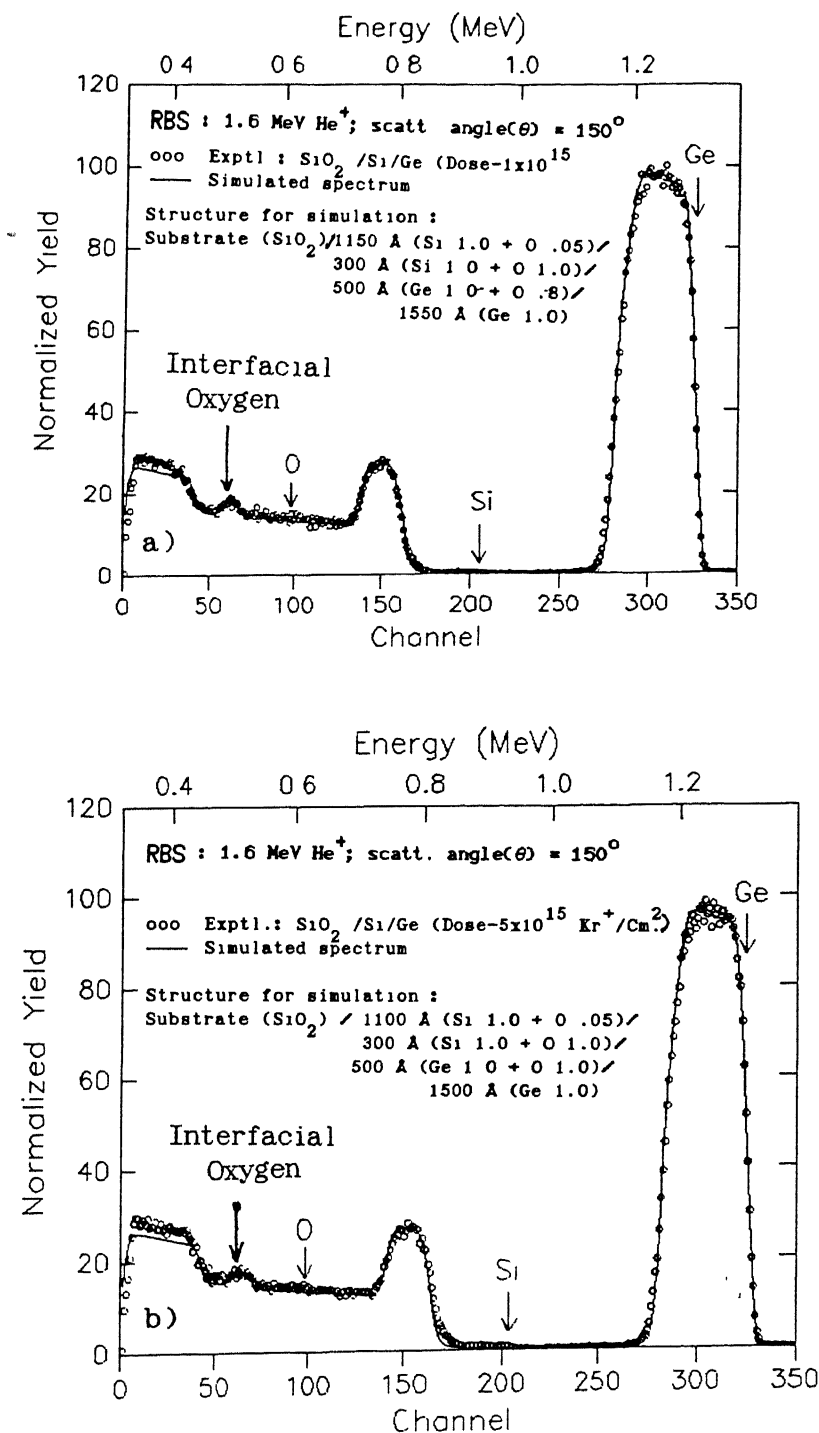
Fig. 3.10 RBS spectra of $SiO_2/Si/Ge$ a)   Dose- 1×10^{15} Kr^+ ions/cm^2
                                             b)   Dose- 5×10^{15} Kr^+ ions/cm^2.

Fig. 3.11   RBS spectra of SiO_2/Si/Ge   a)   Dose- $1x10^{16}$ Kr^+ ions/cm^2
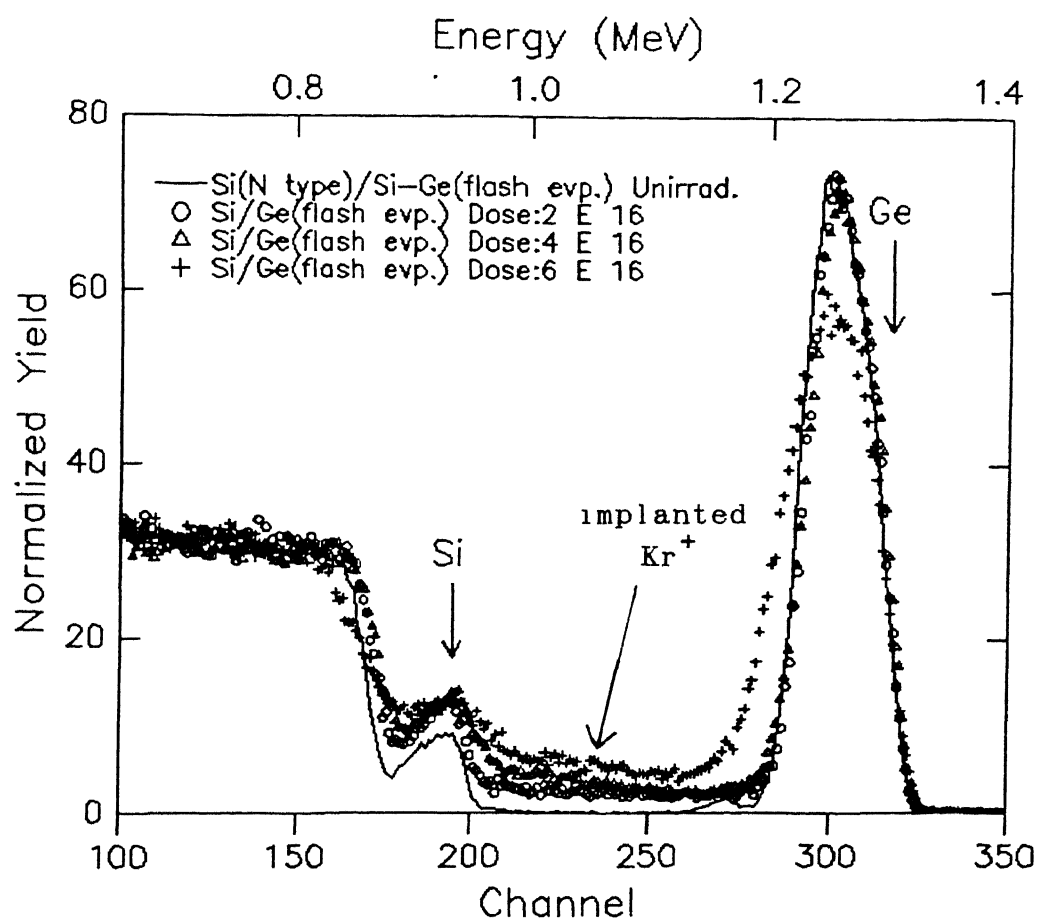
b)   Dose- $5x10^{16}$ Kr^+ ions/cm^2

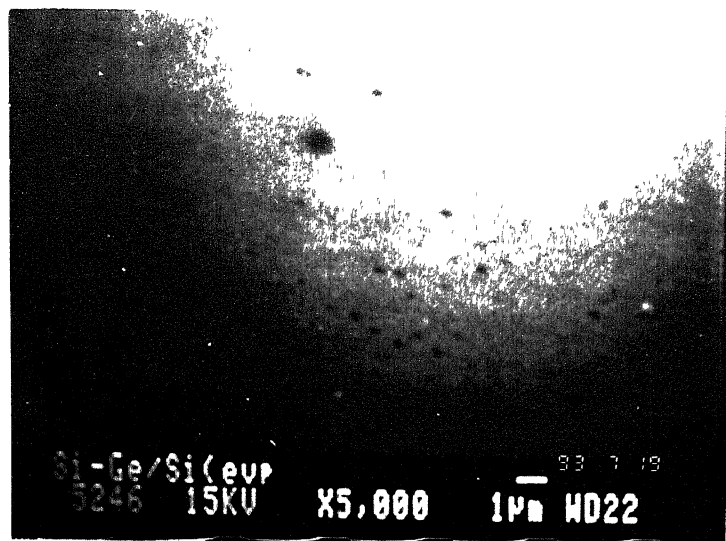Fig. 3.12 RBS spectra of Si/Si-Ge flash evaporation system
at different doses.
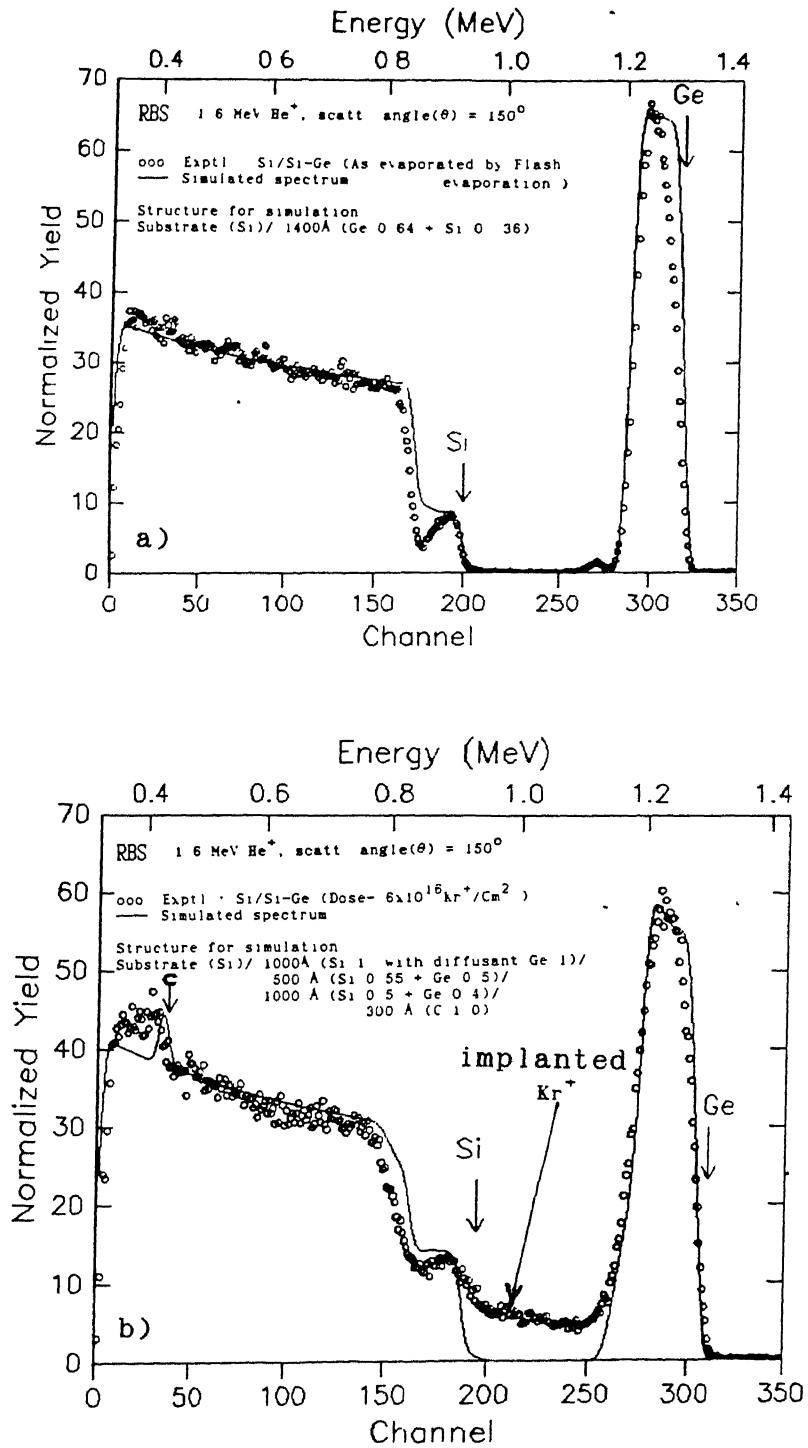
Fig. 3.13 Experimental and simulated RBS spectra of Si/Si-Ge sample prepared by flash evaporation

a) As evaporated ⟶
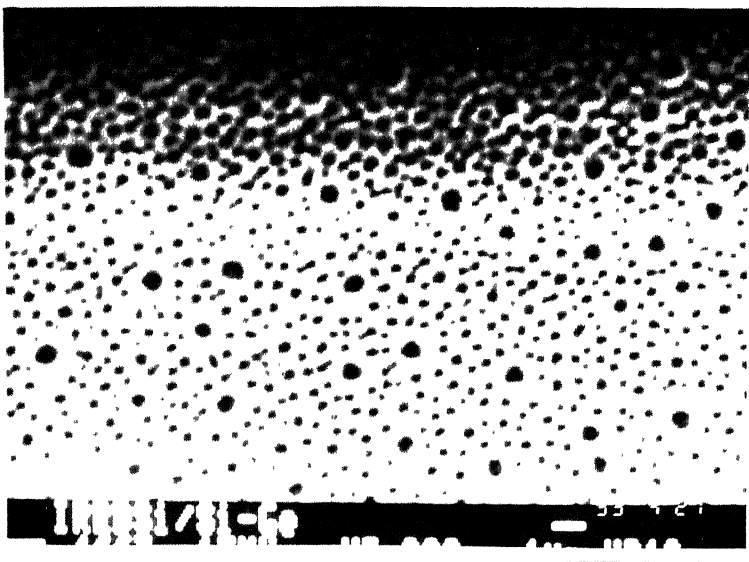
⟵ b) After 4×10^{16} Kr$^+$/cm^2
irradiation

c) After 6×10^{16} Kr$^+$/cm^2
irradiation ⟶
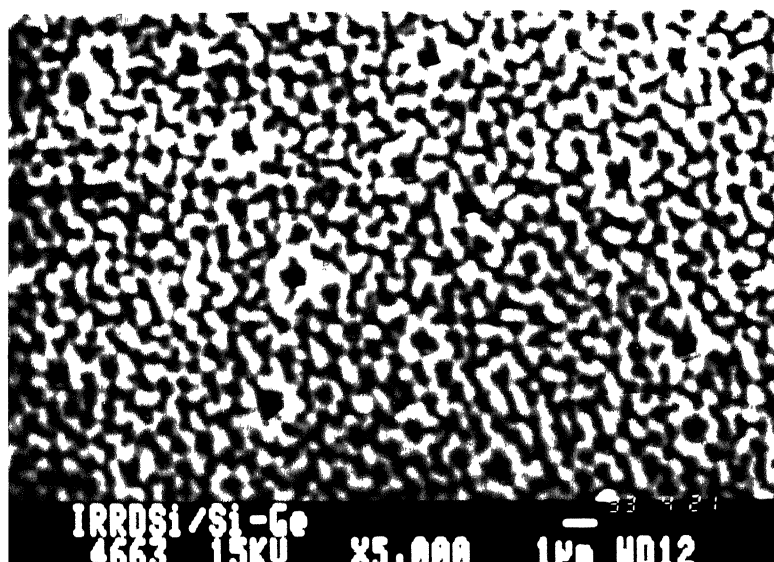
Fig. 3.14 SEM Photographs of Si/(S₁+Ge) sample prepared by
Flash evaporation technique.

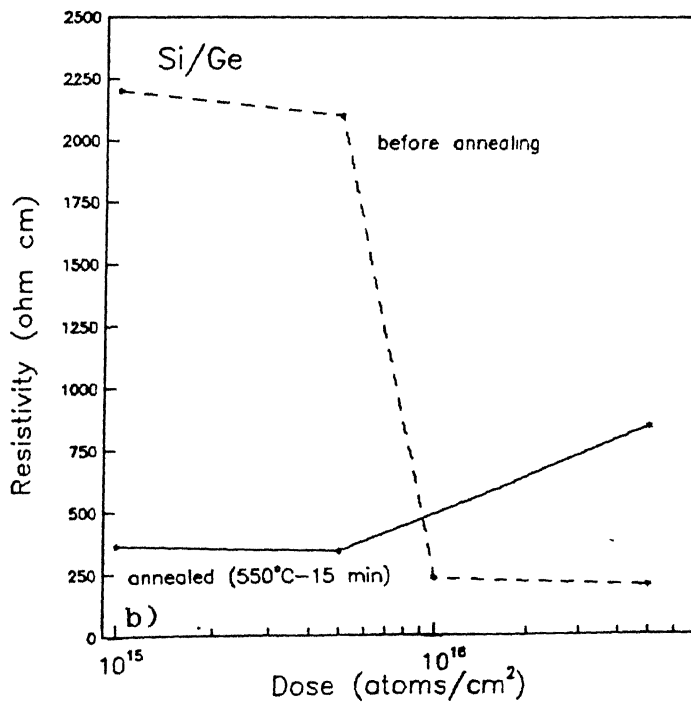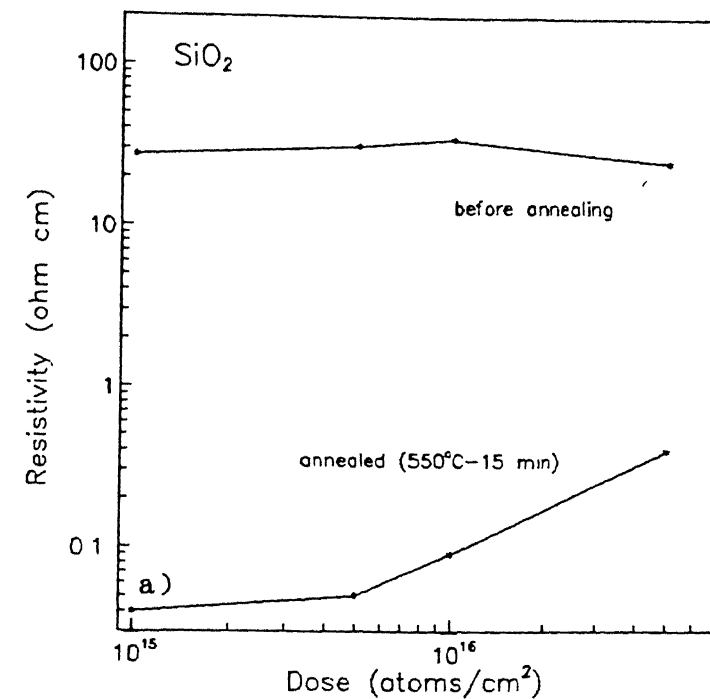Fig. 3.15   Resistivity versus dose of

a) Sample SiO$_2$/Si(1100 Å)/Ge(1400 Å)

b) Si/Ge(1100 Å)

TRIM 91 (91.14)

ION TYPE ^{84} kr^+

ION ENERGY   1 MeV

TARGET LAYERS	Depth	Density
Ge	1550A	5 338
Si	1μm	2.321

ION COMPLETED = 1114

	Range	Straggle
Longitudinal -	5184A	1752A
Lateral Proj. -	1120A	1432A
Radial -	17804A	988A
Vac/Ion -	7448.8	

ENERGY LOSS(%)	Ions	Recoils
Ionizations -	32 34	30 78
Vacancies -	0 06	1 45
Phonons -	0 20	35 23

ION RANGES

Ion Range= 5184A   Skewness = -0.5449
Straggle = 1752A   Kurtosis = 3.0695

a)

0   — Depth ——>   1 5μm

TRIM 91 (91.14)

ION TYPE ^{84} Kr^+

ION ENERGY   1 MeV

TARGET LAYERS	Depth	Density
Ge	1100A	5 338
Si	1 μm	2.321

ION COMPLETED = 203

	Range	Straggle
Longitudinal -	5579A	1535A
Lateral Proj. -	1084A	1381A
Radial -	1682A	965A
Vac/Ion -	6825.1	

ENERGY LOSS(%)	Ions	Recoils
Ionizations -	34 34	31.69
Vacancies -	0.06	1 32
Phonons -	0 21	32 39

ION RANGES

Ion Range= 5579A   Skewness = -0.5912
Straggle = 1534A   Kurtosis = 3.5065

b)

0   — Depth ——>   1 5μm
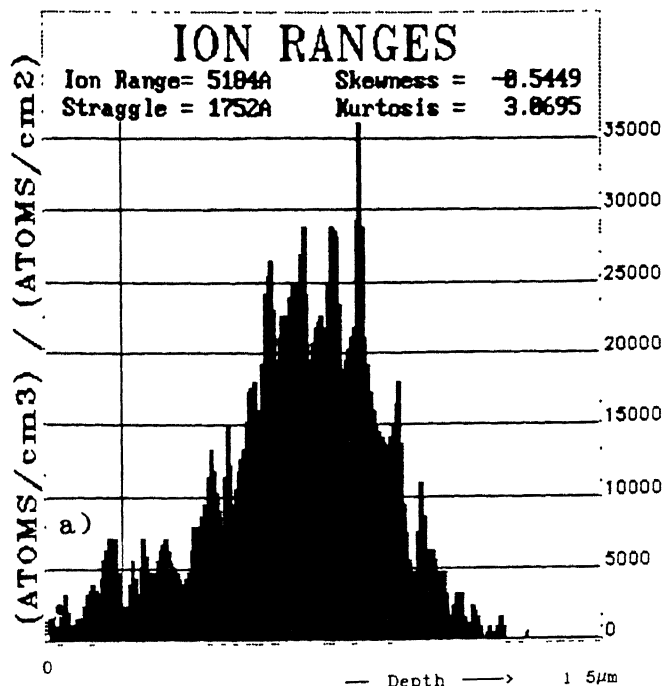
Fig. 3.16 TRIM plots of Kr^+ ion range in sample

a) Si (substrate)/ Ge (1550 Å)

b) Si (substrate)/ Ge (1100 Å)

TRIM 91 (91.14)

ION TYPE   84 Kr+

ION ENERGY   1 MeV

TARGET LAYERS	Depth	Density
Ge	1550A	5 338
Si	1µm	2 321

ION COMPLETED = 1114

	Range	Straggle
Longitudinal	– 5184A	1752A
Lateral Proj	– 1120A	1432A
Radial	– 17801A	988A
Vac/Ion	– 7448.8	

ENERGY LOSS(%)	Ions	Recoils
Ionizations	– 32 34	30 78
Vacancies	– 0 06	1.45
Phonons	– 0 20	35 23

COLLISION EVENTS
Target Displacements
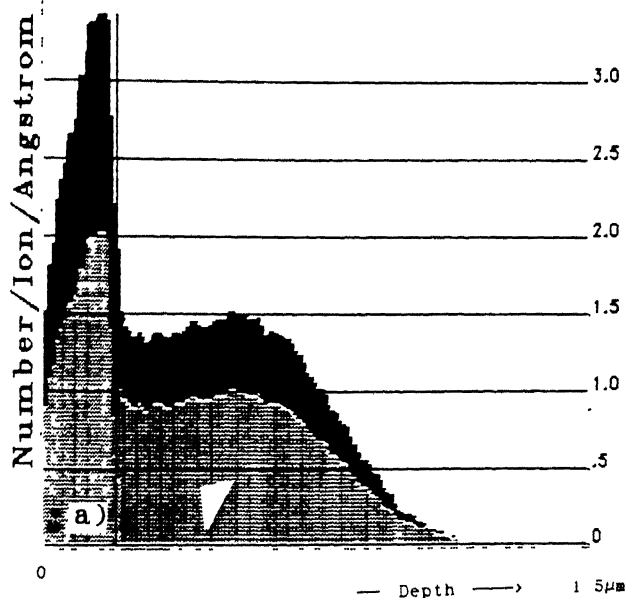
TRIM 91 (91.14)

ION TYPE   84 Kr+

ION ENERGY   1 MeV

TARGET LAYERS	Depth	Density
Ge	1100A	5 338
Si	1 µm	2 321

ION COMPLETED = 203

	Range	Straggle
Longitudinal	– 5579A	1535A
Lateral Proj.	– 1084A	1381A
Radial	– 1682A	965A
Vac/Ion	– 6825.1	

ENERGY LOSS(%)	Ions	Recoils
Ionizations	– 34 34	31.69
Vacancies	– 0.06	1.32
Phonons	– 0 21	32.39

COLLISION EVENTS
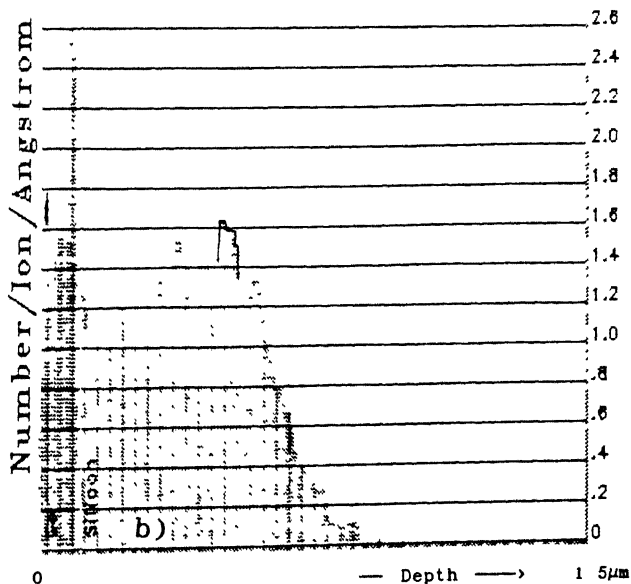### Target Displacements

Fig. 3.17   TRIM plots of collision events (target displacements)

a) Si (substrate)/ Ge (1550 A)
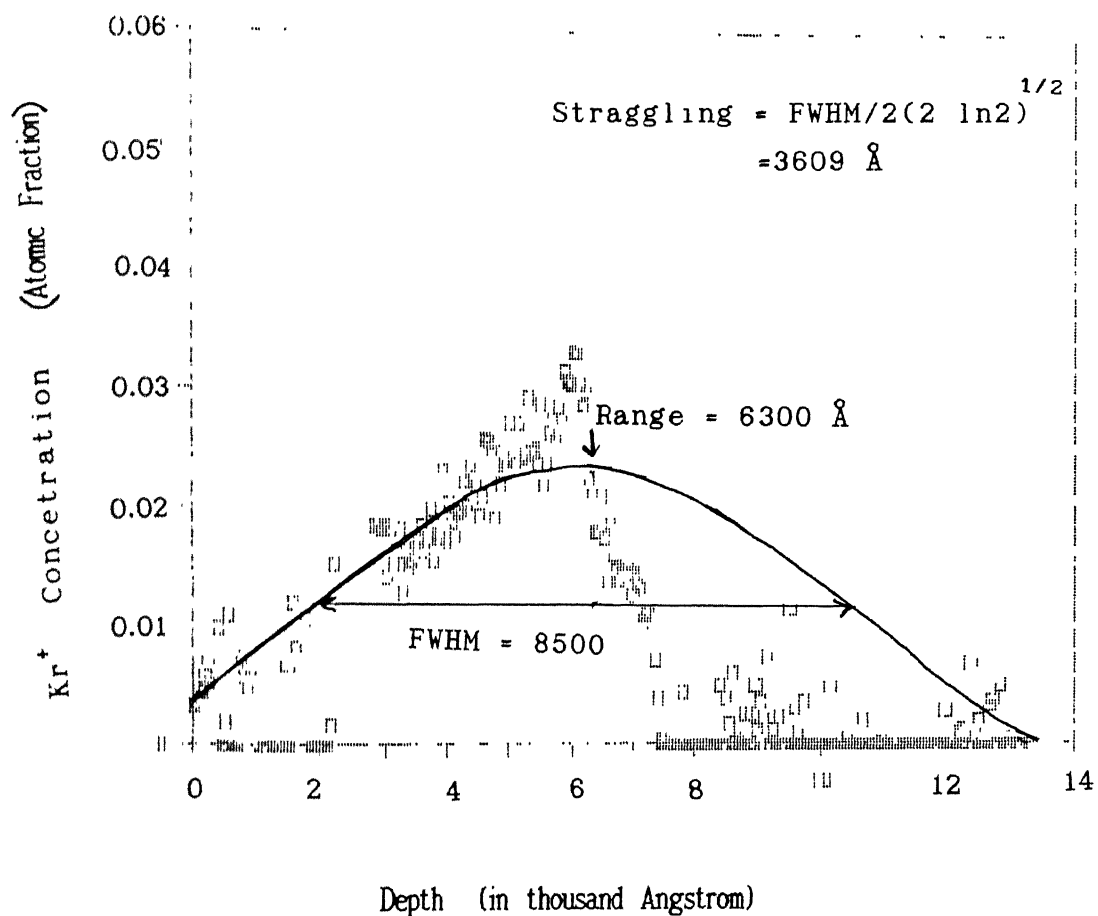
b) Si (substrate)/ Ge (1100 A)

Fig 3.18   Depth Vs. Concentration of Kr (in atomic fraction)
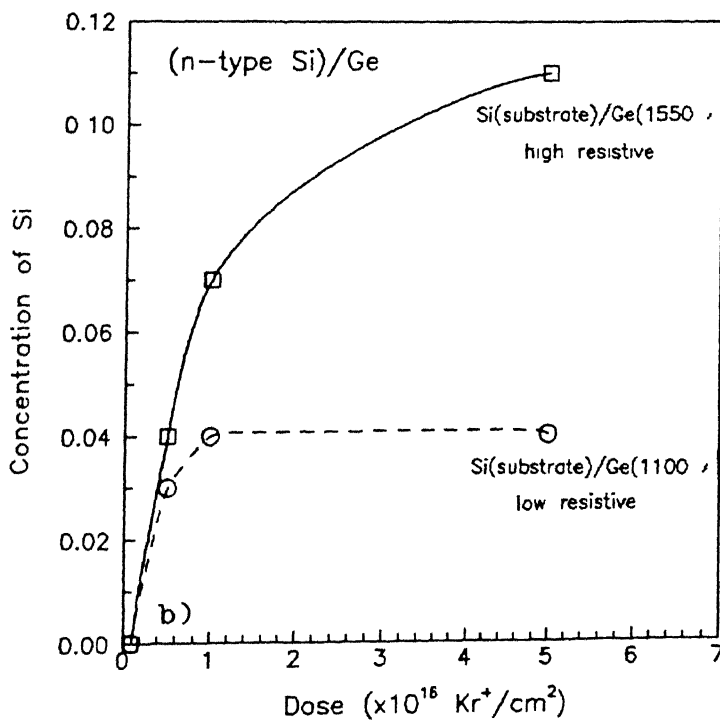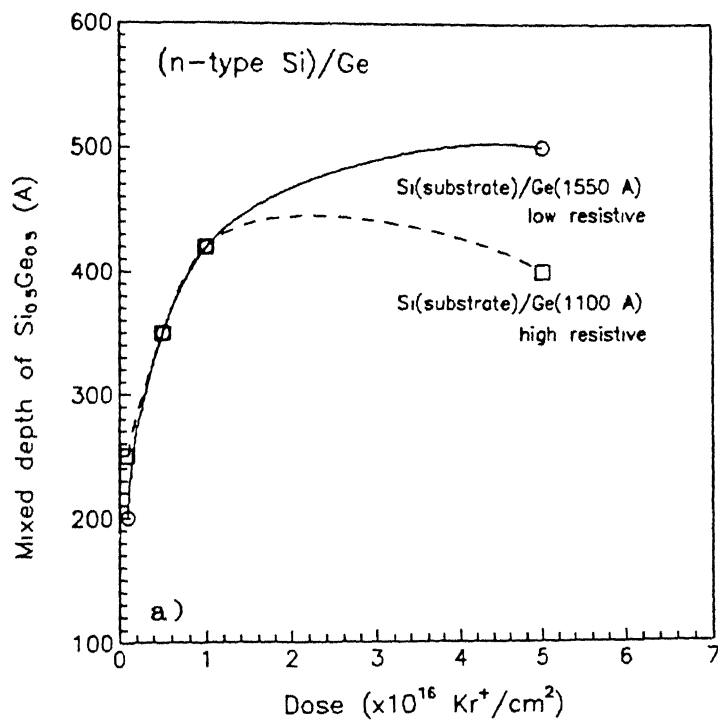in the Si/Ge(1550Å) sample.

Fig. 3.19   a) Mixed depth of $Si_{.5}/Ge_{.5}$ of Si/Ge sample.

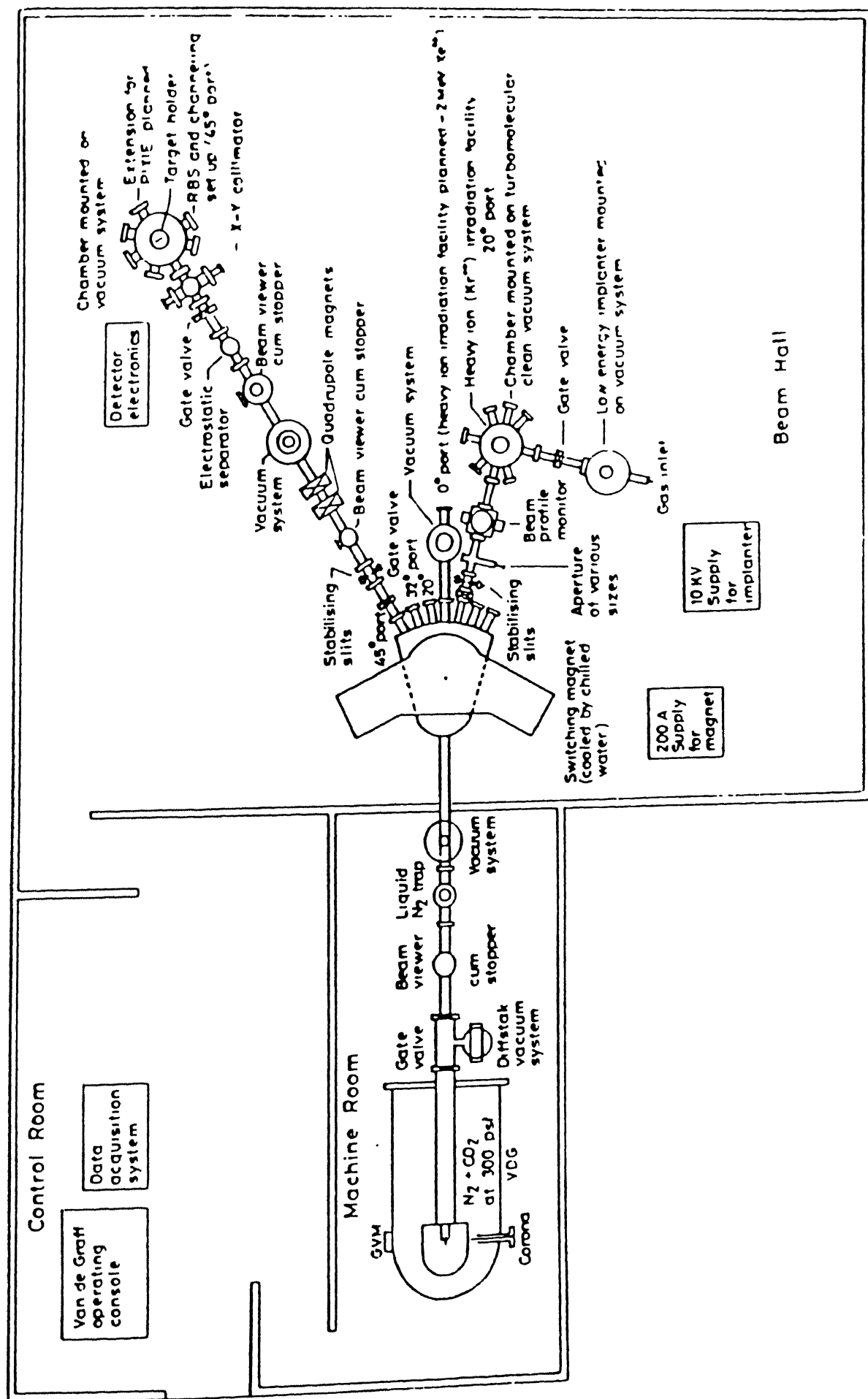b) Concetration of Si on the top layer versus Dose.

Fig.A.1   Layout of the Van de Graff accelerator facility at the
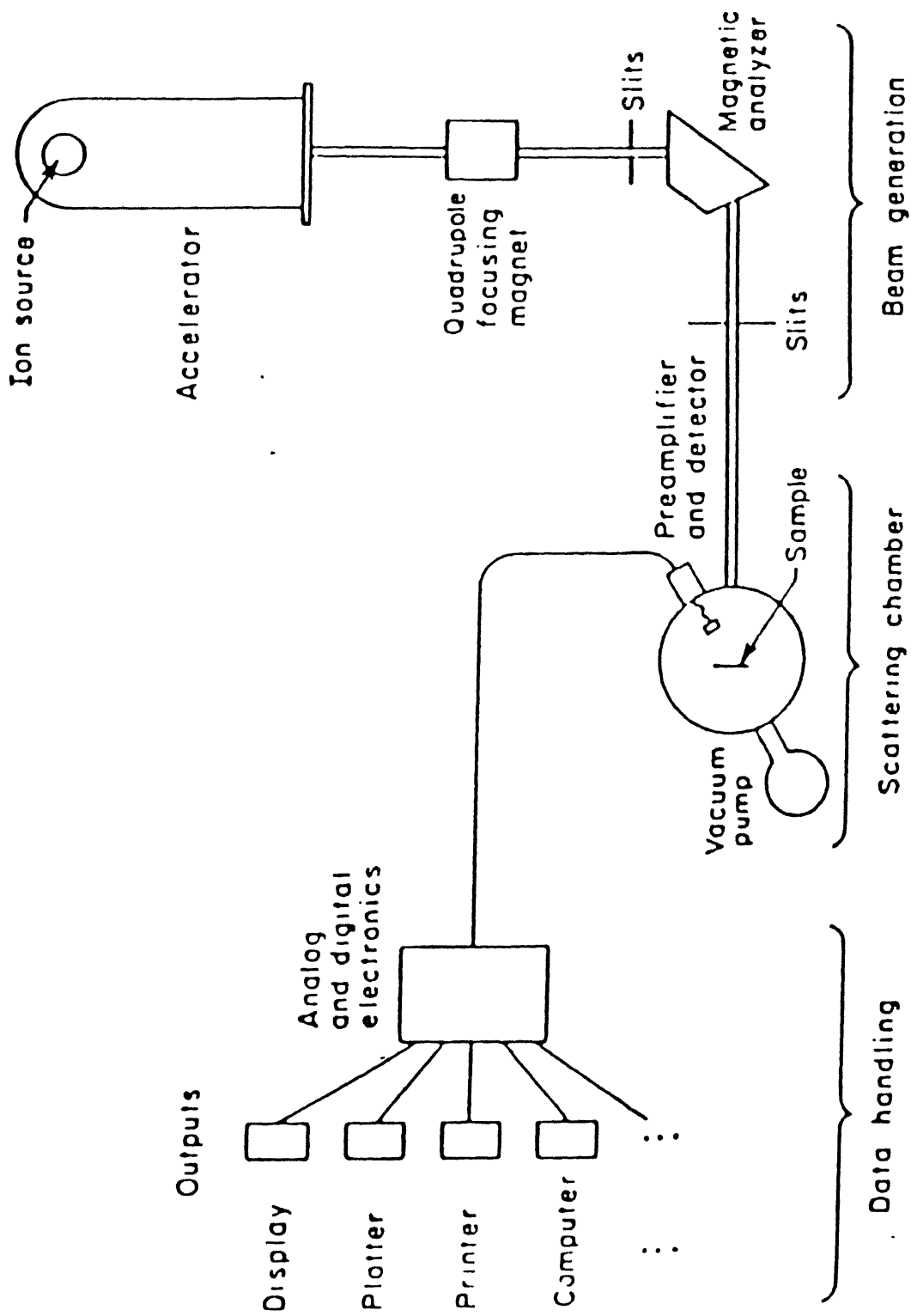Central Nuclear Laboratory, I I T -Kanpur.

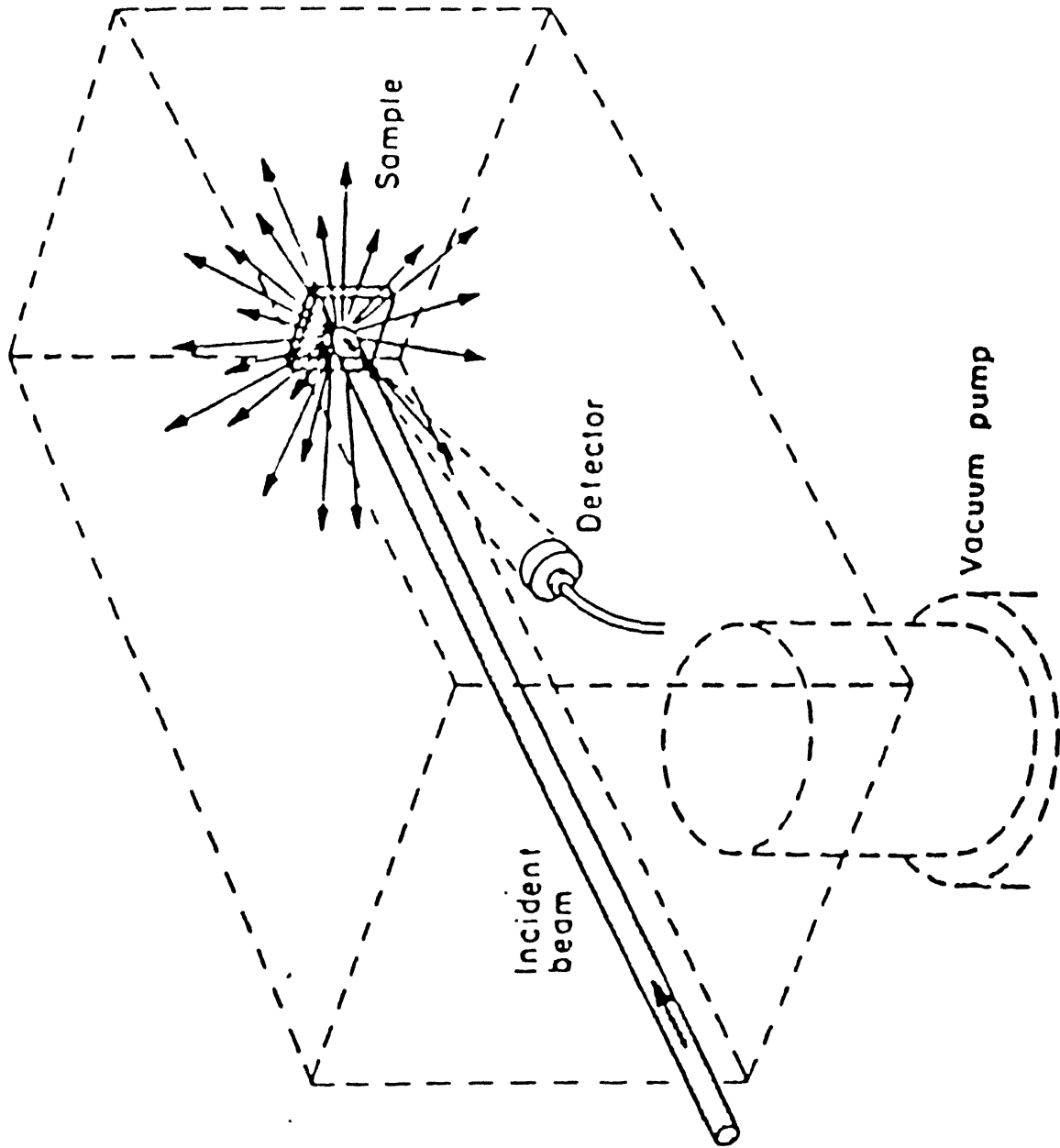FIG B-1 Schematic diagram of a typical backscattering spectrometry system in use today.

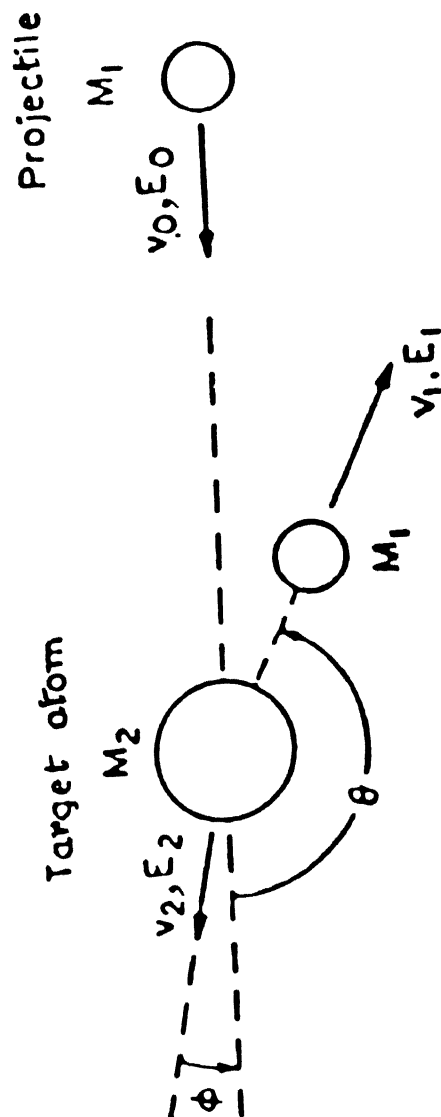Fig. B-2   The scattering chamber in a backscattering spectrometry system.

FIG B-3 Schematic representation of an elastic collision between a projectile of mass M_1, velocity v_0, and energy E_0 and a target mass M_2 which is initially at rest.

REFERENCES

[1]   W. K. Chu, J. W. Mayer and M. A. Nicolet, "Backscattering spectrometry" (Academic Press New York, 1978)

[2]   "Surface Alloying by ions. Electrons, and Laser Beams" (American Society for metals), Edited by L. E Rehn, S T Picran H. Wiedersich.

[3]   R. S. Everback, L. J. Thompson, J. Moyle and Schalit J. Appl.Phys. 53(3), March 1982.

[4]   Z.L.Liau, J.W.Mayer, J. Vac. Sci. Tech., $\underline{15}$(5) (1978).

[5]   R. Pradhan "Study of 1 MeV Kr^+ ion induced mixing at the interface of Tellurium thin film evaporated on Zinc substrate" (M.Tech Thesis).

[6]   B.M.Paine, R.S.Averback, Nucl. Instrum. Meth. Phys. Res., $\underline{B7/8}$, 666-675 (1985).

[7]   S.Matteson, B.M.Paine, M.G.Grimaldi, G.Mezey, M-A.Nicolet, Nucl. Instrum. Meth. Phys. Res., $\underline{182/183}$, 43 (1981).

[8]   B.Y.Tsaur, S.Matteson, G.Chapman, Z.L.Liau, M-A.Nicolet, Appl. Phys. Lett., $\underline{35}$, 825 (1979).

[9]   S.Matteson, B.M.Paine, M-A.Nicolet, Nucl. Instrum. Meth. Phys. Res., $\underline{182/183}$, 53 (1981).

[10]   A.A.Galuska, Nucl. Instrum. Meth. Phys. Res., $\underline{B47}$, 7-14, 1990

[11]   K.Hohmuth, B.Rauschenbach. Nucl. Instrum. Meth. Phys.Res., $\underline{B46}$, 276-283 (1990).

[12]   R.People, J.c.Bean Appl Phys Lett. 48, 538, (1986).

[13]   Cris G. Van De walle, R.M.Martin Phys.Rev.B 34, 5621,1986).

[14] Yia Chung, A. E.Chiov, M.Khoshnevissan J. Appl. Phys. 71, 1349, (1992) & reference there in.

[15] R.A.Soref, F.Namver, J.P.Lorenzo Opt. Lett. 15, 270, (1990).

[16] H.Temkin. T.P.Pearsall, J.C.Bean R.A.Logan, A.S.Lurji Appl. Phys. Lett. 48. 963, (1986).

[17] R.Zachai, K.Eberl, G.Absteiter Phys. Rev. Lett. 64,1055, (1990).

[18] B. Zhu et.al Nucl. Instrum. Meth. Phys. Res., B64, (1992).

[19] Jian Li et al Nucl. Instrum. Meth. Phys. Res., B59/60, (1992).

[20] H.Stohr and W.Klemm Z.anorg. Chem.,241,1939,305 323.

[21] 'Material Science and Engineering' by V. Raghavan.

[22] K. Sarvanan "Damage and annealing studies of 1 MeV Kr[++] implantation in heavily doped silicon." (M.Tech. thesis)

[23] D. K. Schroder "Semiconductor Material and device characterization". (A Wiley Interscience Publication).

[24] G. Dearnaley, J. H. Freeman, R, S, Nelson and J. stephen "Ion Implantation". (North Holland Publication).

[25] J. Biersck and L Hoggmark, Nucl. Instrum. Meth. Phys. Res., Vol 174, 257 (1980).

[26] 'The stopping and range of ion in solids' By J.F.Ziegler, J.Biersack and U.littmark, Pergaman Press, New York 1988.

[27] N Banerjee 'Atomic diffusion and phase precipitation studies in amorphous metallic alloys using RBS and Mossbauer spectroscopy. (Ph.D thesis).

[28] R.J.Schrentelkamp et.al. Nucl. Instrum. Meth. Phys. Res., B84, 448, (1990).

[29] "Ion Beam Handbook For Material Analysis" edited by J.W.Mayer, E.Rimini, Academic press.

[30] "Fundamentals of Surface and Thin Film Analysis by L.C.Fledman, James W.Mayer, North-Holland.